Master of Science Thesis

Diffusion q-space measurements *in-vivo*: does sequence timing influence the result?

Emil Nordh

Supervisors:
Sara Brockstedt and Jimmy Lätt

Medical Radiation Physics
Clinical Sciences, Lund
Lund University, 2007

Abstract

Magnetic resonance imaging (MRI) is still a fast growing area of research and is an important part of the clinical tools used for diagnosis of various diseases. The diagnostic values of diffusion imaging are well known especially for ischemic stroke in the acute phase.

This work concerns whether the apparent diffusion coefficient (ADC) and the full width at half maximum (FWHM) changes when the imaging protocol changes e.g. when the diffusion time or the duration of the diffusion encoding gradient duration, δ, changes.

All measurements were performed *in-vivo* using either on a Siemens Allegra 3T head scanner or a Philips Achieva 3T whole body system.

The result of varying the different diffusion time shows that FWHM in of the probability distribution in white brain matter increases linearly in the direction parallel to the fibre structure, as expected from Einstein's equation. Whereas in the direction orthogonal to the fibres FWHM is increases only slightly and this is assumed to reflect the restriction of the diffusion in this direction. The FWHM in grey brain matter shows the same tendency to increase as for the parallel direction in white brain matter.

When the duration of the diffusion encoding gradients, δ, is increased, simulations indicate that both ADC and FWHM should decrease. This was verified in the *in-vivo* measurements although the decrease in the orthogonal direction was smaller than expected.

In most of the literature today it is assumed that the ADC and the FWHM values are independent of the duration of the pulsed gradients. The result presented in this work suggests that this assumption should be reconsidered.

Content

1 Introduction

In 2003, Paul C Lauterbur, USA, and Sir Peter Mansfield, England, received the Nobel Prize in medicine for an invention they made during the 1970s. Lauterbur was awarded the prize for the method of image reconstruction based on magnetic field gradients and Mansfield for the echo planar imaging (EPI) readout technique. Their innovation led to a new non-invasive method to examine the inner structures of the human body *in-vivo*. The first commercial equipment was in use in the early 1980s and in 2002 there were over 22 000 scanners in use around the world [1]. In the specific area of diffusion MRI, Richard R. Ernst has contributed a great deal and he was awarded the Nobel Prize in 1991 for the work regarding the nuclear magnetic resonance (NMR) spectroscopy. In the early 1990:s the first clinical application of diffusion weighted images (DWI) was discovered and the diagnosis of ischemic stroke in the acute phase was made possible [2]. Today the diffusion imaging technique is used as an important diagnostic tool, not only for acute ischaemic stroke but also for brain tumours, Multiple Sclerosis, Alzheimer's disease etc.

The MR technique of today is used both in the field of chemical research and in medical diagnostic imaging, however the equipment used in the two areas differs. NMR is used for investigation of structures and compositions whereas MRI is a non-invasive method that takes images of the inside of the body and is used for clinical diagnosis all around the world. The NMR scanner has a higher magnetic field strength and stronger gradients than a clinical scanner, however, the bore size of a NMR spectrometer is in the order of mm and only allows studies of small test samples whereas the MRI scanner has a bore size large enough to fit a human body.

The random, Brownian motion, of water molecules can be measured by diffusion weighted MRI, a technique that is based on the phenomena of signal attenuation due to phase dispersion. The diffusion motion is dependent of the temperature and the viscosity of the fluid.

The logarithm of the diffusion weighted signal can be plotted against the strength of the diffusion encoding (b-value) and hence results in a signal attenuation curve. The slope of this logarithmic curve is the apparent diffusion coefficient (ADC) value, that is the speed of the diffusion measured in m^2/s. Recently the signal attenuation was found to be multi-exponential and hence, the ADC has be divided into to parts, ADC_{fast} and ADC_{slow} [4]. ADC_{fast} is the initial slope of the signal attenuation curve and ADC_{slow} is the slope of the more slowly decaying part of the curve. Using only low b-values, up to approximately 2000 s/mm^2, the diffusion signal decay is mono-exponential and the ADC values can be estimated with a linear regression, but if high b-values are used a bi-exponential function provides a better fit [3], [4]. By using a linear approximation of ADC_{fast} and ADC_{slow} the ADC values are under- and overestimated, respectively, relative to the bi-exponential fitting method [5]. A problem regarding ADC values is that there are no consensus within the scientific community what ADC_{fast} and ADC_{slow} really is describing. A theory supported by Assaf *et al.* [6] and van Zijl [7] is that the ADC_{fast} corresponds to the intra cellular fluid water whereas others describe it

like just the opposite, Sotak [8]. In one study, Schwarcz *et al.[9]*, discards the idée that ADC_{fast} and ADC_{slow} corresponds to be different cell compartments and says that we are just measuring a combination of the both components. The conclusion was made after conduction of two different experiments, the first where conducted on 27 mail mice where a global ichemia was induced using a cupper rod cooled in liquid nitrogen applied to the scull of the mice for 10 s. The cell membrane was partly or fully disintegrated and the extracellular space were incorporated in the intracellular space. In the second blood from healthy human volunteers was centrifuged so that the extra cellular space between the erythrocytes was negligible. The conclusion of the study was that ADC_{fast} and ADC_{slow} not corresponds to any particular part of the cells matrix.

An alternative way of analysing the diffusion is to perform so called q-space imaging, where the signal attenuation curve is Fourier transformed, resulting in a probability density distribution function. The width at half of the maximum (FWHM) of the distribution will be an estimation of the mean displacement of the water molecules and this can be taken as a measurement of the averaged net distance the water molecules have moved during the diffusion time. In the case of restricted motion the FWHM will not increase with increasing diffusion time, T_d, (the waiting time when the molecules can move around, diffuse) [3], but will reach a value which is proportional to the structural confinement [10].

A problem when performing diffusion measurements is the fact that the duration of the diffusion encoding gradient, δ, isn't infinitely short, the water molecules is moving during the encoding phase. To avoid this the short gradient pulse (SGP) approximation must be valid and $\delta D << a^2$ where a is the confinement size and D is the diffusion coefficient. SGP approximation means the water molecules cant reach the confinement during the duration δ.

1.1 Purpose

The purpose of this study was to evaluate the possibilities to perform q-space imaging *in*-vivo using clinical MRI scanners and to examine if and how the FWHM is affected when the diffusion time is altered and also to investigate how $ADC_{lin\text{-}fast}$ and FWHM changes when the SGP approximation is violated. A better understanding of how different protocol parameters affect the measurements can improve protocol optimisation and also provide a more accurate reading of the images.

1.2 Overview of the current state of diffusion MRI and NMR

In the early 80:ties, before the clinical use of DWI was possible, Wesbey *et al.* performed the first measurement of molecular self-diffusion with MRI [11]. The diffusion encoding of the molecules was preformed only by varying the amplitude of the slice selection gradient and not, like today with separate diffusion encoding gradients. The great advantage of diffusion measurements with MRI according to Weseby *et al.* was the possibility to measure several samples as in the case of measurement carried out with the NMR spectrometer.

In 1985 Le Bihan and Breton [12] presented a work that simplified the method that was originally described by Stejskal-Tanner in 1965. Le Bihan and Breton presented a more direct method for diffusion measurements and introduced the notation of the gradient factor b, which simplified the determination of the relationship between the diffusion encoding and the diffusion coefficient. In 1986, Le Bihan *et al.* introduced the term ADC [13] that takes restricted diffusion into account and also the time period for which the diffusion is observed. The term "apparent" comes from the fact that the diffusion coefficient measured *in-vivo* deviate from the theoretical diffusion coefficient. The difference is contributed to the fact that when the diffusion coefficient is measured *in-vivo*, effects from cell membranes and cell elements as well as the perfusion related pseudo diffusion will cause the value of the diffusion coefficient to deviate from the theoretical value of water.

In 1991 Callaghan *et al*. [14] made a NMR study on porous alumina saturated in water and in decane and on Bentheimer sandstone. Both samples were cylinders of 1.5 cm in length and 0.7 cm in diameter. The experiment was carried out as a function of the magnitude of q (approximately proportional to the square root of b) and the echo amplitude was plotted as a function of the Δ. Callaghan et al. did show that when Δ increases, from a few to a few hundred milliseconds, the collisions with the pore walls reduce the effective rate of diffusion, leading to a reduction in the slope of each curve and thereby a reduction in the ADC value.

More recently several groups have examined the effects on the FWHM when changing the T_d. Nossin-Manor *et al.* [15] performed an experiment on extracted rat spinal cord (SC) with in an NMR spectrometer where they concluded that the white matter (WM) *vs.* grey matter (GM) contrast increase when the T_d increase. This effect is only noticeable in the direction perpendicular to the long axis of the SC. In the parallel direction the contrast was not affected by the choice of the T_d. They also found that the increase of the mean displacement was less in the direction perpendicular to the SC in WM than in GM when the T_d was increased. In the same study they performed an experiment where δ was changed from 2 ms to 20 ms. They concluded an increase in the probability of zero displacement and a decrease in the mean displacement (proportional to FWHM).

Topgaard and Söderman [10] have examined the effect on the root mean square (rms) displacement for extremely short T_d (much shorter than what can be obtained with MRI) for restricted diffusion and found that for the shortest time the rms displacement follows that of free water but when the T_d increase further the rms displacement becomes constant. The measurements were performed with a NMR spectrometer on a water film with a thickness of approximately 50 µm. For the shorter T_d:s the molecules will appear to be free since they do not bounced into the walls. When the T_d is increased the restriction, made out of the walls, will stop the spread of the molecules and the rms will become constant.

On the same topic but in a different field of research Wassenius *et al.* [16], have examined oil filled polystyrene spheres with an average radius of 1.5 µm with a NMR self-diffusion measurment technique. Their results show that the rms distance of oil particles inside the

spheres is practically constant for different T_d:s, while the rms from the particles itself follows the behaviour of a free particle.

The effects on different parameters when changing duration of the diffusion encoding gradient pulse, δ, has been made by several groups. Mitra and Halperin presented a theoretical work about the Centre of Mass (COM) theory [17]. Their work explains what happens to water molecules in pores during the duration of the diffusion gradient. The COM of the path of a water molecule during a specific time will move towards the middle of the confinement when the gradient pulse time increases. Mitra and Halperin conclude that if δ is infinitesimal short a particle will not move during δ and the COM will be the location of the particle. If the time δ increases the measured pore size will be smaller than the actual pore size and the effect of COM will effect the measurement. If the gradient duration is increased even further, the pore space (the space where the pores are located) will appear uniform since the water molecule will escape the pore through the semi permeable membrane.

Malmborg *et al.* [18] performed an experiment on a water-in-oil emulsion in order to investigate what happens when the SGP approximation is violated on an NMR scanner. The result of the study, where they were measuring on molecules within oil droplets, was that if the SGP approximation is violated the measured pore size will be considerably smaller than the actual pore size. If the mean square distance (MSD) is of the same magnitude, or larger, than the pore size the information about the pore size will gradually be lost for increasing δ. As an example they measured a decrease of one order of magnitude in MSD when δ is changed from 1.5 to 50 ms. In 2006 Malmborg *et al.* [19] presented the results of a study where they investigated the breakdown of the SGP-approximation. In this study they used an oil-water-salt emulsion, where the salt was confined to the pores and the water and the oil is moving freely. The result was a small decrease in FWHM, when varying δ, in a salt solution where the diffusion is limited by the droplet size. For the oil and water, where the diffusion not is limited, the rms displacement was constant.

The above described studies have one thing in-common; they were all performed *in-vitro* on NMR spectrometers. In an NMR system the gradient strength is larger and the bore size is smaller then in an MRI scanner. Hence NMR studies are only possible on very small samples in test tubes and can not be performed *in-vivo*. Due to the higher performance of the NMR system it will show less uncertainty in the measuring points and this will increase the probability to observe differences in ADC and FWHM. But will the violation of SGP have effects on a clinical scanner when used *in-vivo*?

A tensor model were a number of different diffusion directions is combined to form a tensor, was proposed by Assaf *et al.* [20]. The tensor approach gives us a value of FWHM that is independent of the direction.

2 Diffusion MRI Theory

2.1 Self diffusion

The self-diffusion is the random motion that originates when the molecules collide with other molecules. The motion is called a Brownian motion and can be described by a Gaussian probability density function.

Self-diffusion is caused by thermal mobility of the molecules. The Brownian motion of the molecules occurring due to their thermal energy motion is described by the displacement probability which is defined as $P(s,t)$ where P is the probability to find a particle at a certain place after a certain time, the variable s is the displacement and t is the time interval. The change in probability as a function of time, in three dimensions, can be written like

$$\frac{\partial P}{\partial t} = D\nabla^2 P \qquad \textbf{Eq. 1}$$

where D is the temperature dependent diffusion coefficient [$m^2 s^{-1}$].

If the molecules are free there motion are not subject to any restrictions and for a free particle the mean-square displacement is given by

$$\left\langle s^2 \right\rangle = 2nDT_d \qquad \textbf{Eq. 2}$$

where n is the number of dimension (1, 2 or 3) and T_d is the diffusion time [6].

2.2 Diffusion weighting

2.2.1 Diffusion weighted imaging – DWI

The diffusion weighting (DW) gives information of the mobility of the water molecules.

In 1965 Stejskal and Tanner introduced a pulse sequence suitable for diffusion measurements, see Figure 1, [24] and together with this pulse sequence they also introduced their famous equation which was later simplified by Le Bihan and Breton in 1985 [12]

$$S(b) = S(0) \cdot e^{-b \cdot D} \qquad \textbf{Eq. 3}$$

where *S(b)* is the DW signal and *S(0)* the non-diffusion weighted signal acquired for the same TE. The b-value is the diffusion sensitivity and describes the relationship between the diffusion coefficient, *D*, and the signal attenuation. The b-value is defined by,

$$b = \gamma^2 G^2 \delta^2 T_d \,, \quad \left[s/m^2 \right] \qquad \textbf{Eq. 4}$$

where G is the amplitude of the diffusion encoding gradient and δ is the duration of the gradient pulse, see Figure 1. γ is the gyromagnetic ratio and T_d is the effective diffusion time which is defined as

$$T_d = \Delta - \frac{\delta}{3} \qquad \textbf{Eq. 5}$$

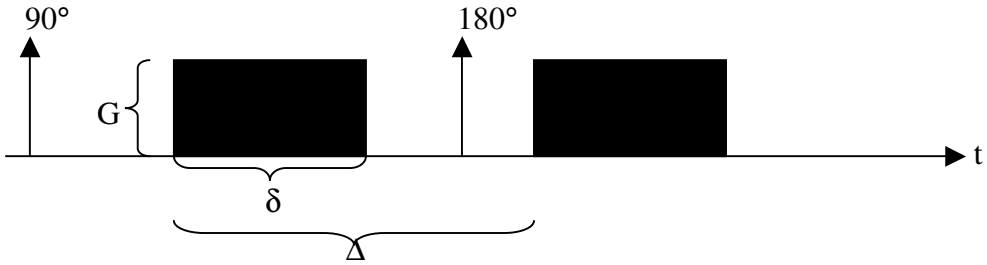

Figure 1 The Stejskal and Tanner pulse sequence, where δ is the duration of the diffusion encoding gradients, G is their amplitude and Δ is the time between the onset at the two separate gradient pulses.

By labelling the water molecule with a phase shift at one time and then wait the T_d before switching on the second gradient the distance can be estimated by the amount of the net phase shift. The net phase shift is dependent upon the net distance the molecules has moved so if the molecules have moved a long distance during the T_d the dephasing will be larger and the net magnetisation vector will decrease due to phase dispersion. If the molecule hasn't moved between the gradient pulses (or returned to the same spot), their phase will be refocused. The net magnetisation will depend on the degree of phase dispersion, i.e. a higher diffusion coefficient will result in a lower net magnetisation vector.

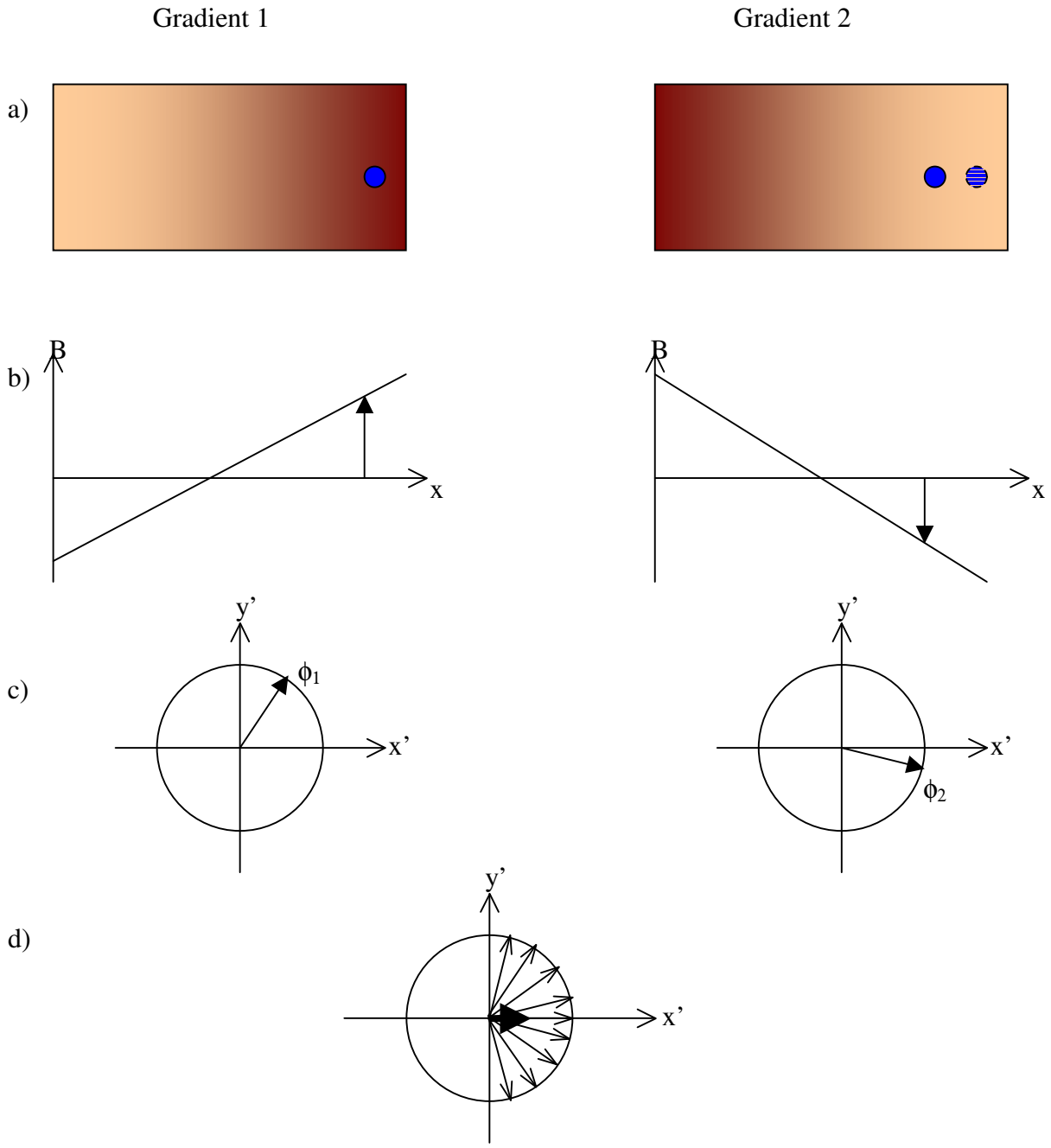

Figure 2 A spin (marked in the left column) is moving from one position to another (marked in the right column) (a). The spin will be affected by the gradients with different polarity and different magnitude (b). The first gradient will create a phase shift, ϕ_1 (left) and the second gradient will create a phase shift in the opposite direction, ϕ_2 (right) (c). In one voxel there are many molecules and if they move the net effect of diffusion will be a dephasing and the net magnetisation vector will decrease when the diffusion increase (d).

2.2.2 Apparent diffusion coefficient – ADC

The ADC is the diffusion coefficient that can be determined from the Stejskal-Tanner equation if at least two different b-values have been measured.

$$D = \frac{\ln\left(\frac{S(b_1)}{S(b_2)}\right)}{b_1 - b_2} \qquad \textbf{Eq. 6}$$

The *in-vivo* diffusion coefficient is denoted ADC since biological effect affects the value.

Recently it has become customary to divide the ADC into two components ADC_{fast} and ADC_{slow}. ADC_{fast} is usually determined as the linear approximation of the first part of the signal attenuation curve, for b-values up to b =2000 s/mm^2 [25] (in the clinic b=0 – 1 000s/mm^2 is often used) and is then called $ADC_{lin\text{-}fast}$, see Figure 3.

When high b-values are included in the measurement the signal decay occurring due to diffusion is no longer mono-exponential [3], [4], but is more accurately described in terms of a bi-exponential function, Eq. 7, [4] or even higher order exponentials.

A linear approximation of ADC_{fast} results in an underestimation of ADC relative to the bi-exponential fitting method and ADC_{slow} results in an overestimation of the ADC values relative to if the bi-exponential fitting method [5].

$$\frac{S(b)}{S(0)} = A_1 e^{-b \cdot ADC_{fast}} + A_2 e^{-b \cdot ADC_{slow}} \qquad \textbf{Eq. 7}$$

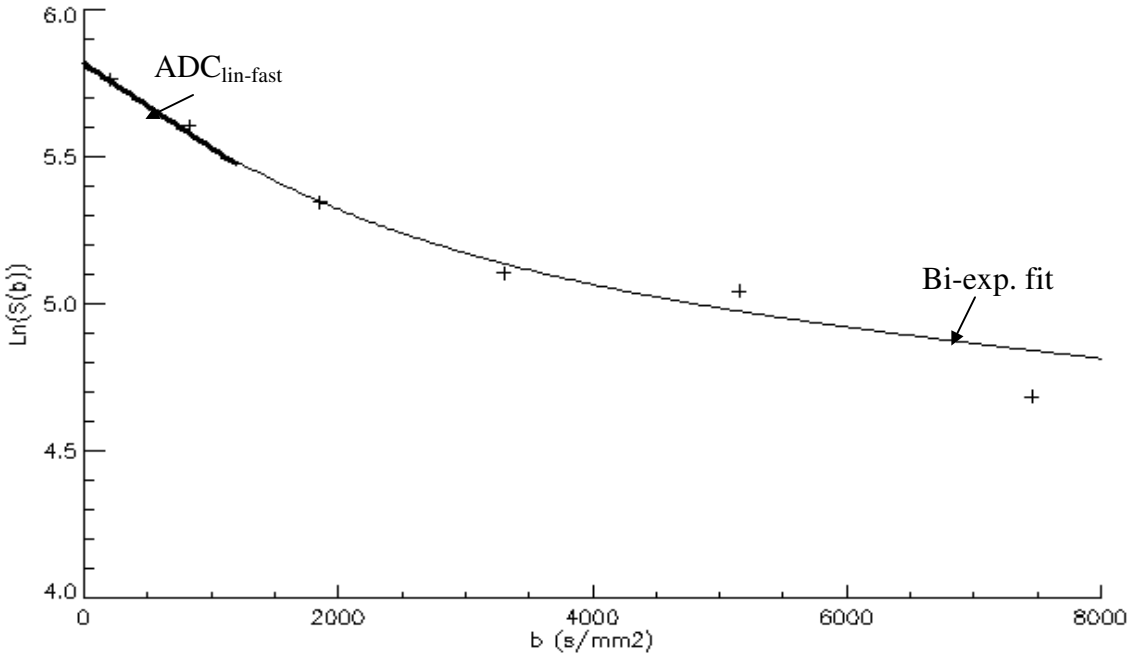

Figure 3 $ADC_{lin\text{-}fast}$ (thick solid lines) is the linear fit to the signal versus b-value attenuation curve. The logarithm of the measured signal values are represented by + and the thin solid line shows a bi-exponential fit to the signal values according to Eq. 7.

2.2.3 Diffusion tensor imaging – DTI

To quantify the diffusion anisotropy one can assume a tensor model and hence perform diffusion tensor imaging (DTI). The advantage is that the tensor is independent of the direction in which the diffusion is measured directions. However, the measurements are not directional independent so the directions have to be chosen in a non-linear way.

To perform DTI diffusion sensitive measurements has to be carried out in at least six non collinear directions and one image with b = 0 s/mm^2 has to be obtained. To the measured ADC values (one in each direction) an ellipsoid is fitted to form the tensor. If the ADC is the same in all directions the tensor will assume the shape of a sphere but if the ADC is restricted or hindered in any or two of the directions the tensor will be described by an ellipsoid.

The diffusion coefficient matrix describes the tensor in the laboratory frame of reference (x, y, z).

$$\mathbf{D} = \begin{pmatrix} D_{xx} & D_{xy} & D_{xz} \\ D_{yx} & D_{yy} & D_{yz} \\ D_{zx} & D_{zy} & D_{zz} \end{pmatrix} \qquad \textbf{Eq. 8}$$

The matrix can be diagonalized and the obtained eigenvalues multiplied by the new base vectors (eigenvectors) is the semi-axis that forms the ellipsoid. The diagonalisation is just a change in base vectors and the eigenvalues is the length of the eigenvectors in that direction, see Figure 4 and Eq. 9.

$$\begin{pmatrix} \lambda_1 & 0 & 0 \\ 0 & \lambda_2 & 0 \\ 0 & 0 & \lambda_3 \end{pmatrix} \begin{pmatrix} e_1 \\ e_2 \\ e_3 \end{pmatrix} \qquad \textbf{Eq. 9}$$

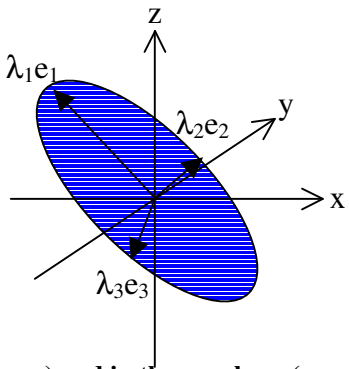

Figure 4 The tensor in the old base (x,y,z) and in the new base (e_1,e_2,e_3). λ_1, λ_2, λ_3 are the eigenvalues and corresponds to the length of the eigenvectors (semi-axis), in the new base, which describes the ellipsoid.

2.3 q-space imaging

The q-space imaging is a supplement to DTI. It is easier to show the bi-exponential signal decays. The signal decay in white matter as been shown not to be mono-exponential at high b-values [3] and in such a case the can the q-space approach be of help.

The q-space approach with high b-values was first used by the chemist in NMR measurements. The measurement is an ordinary DW measurement but with higher sensitivity. and that makes it more easy to identify the bi-exponential decay, Eq. 3, is not valid. The signal attenuation is better described by the bi-exponential approach in Eq. 7 or even a multi exponential decay of the signal curve [3]

$$S(b) = S(0)\sum_{i=1}^{n} A_i e^{-b\cdot D_i} \qquad \textbf{Eq. 10}$$

where n are the number of components and A_i are the relative signal fraction from molecules having the diffusion coefficient D_i.

In q-space imaging the signal can be described as a function of the reciprocal space vector, the wave vector **q** [m^{-1}] defined as

$$\mathbf{q} = \frac{\gamma}{2\pi}\delta\cdot\mathbf{G} \qquad \textbf{Eq. 11}$$

The relation between b and **q** can be determined from Eq. 3 and Eq. 11

$$b = 4\pi^2 q^2 T_d \qquad \textbf{Eq. 12}$$

The loss in signal, *S*, during T_d is due to the phase dispersion created by movements occurring during T_d and can be described by the equation below [26]. The loss in signal is more sever for higher b or q values.

$$S(\mathbf{G}) = \int \rho(\mathbf{r}) \int P_S\left(\mathbf{r}|\mathbf{r}', \Delta\right) e^{i\gamma\delta\mathbf{G}(\mathbf{r}'-\mathbf{r})} d\mathbf{r}' d\mathbf{r} \qquad \textbf{Eq. 13}$$

where $\rho(\mathbf{r})$ is the normalized spin density and $P_S\left(\mathbf{r}|\mathbf{r}', \Delta\right)$ is the average propagator i.e. the probability that a molecule have moved the distance from **r** to **r'** during the time Δ.

By substituting **G** with the expression **q** (Eq. 11) in Eq. 13,the signal can be expressed as a function of **q** and will be an average of net displacement.

$$S(\mathbf{q}) = \int \rho(\mathbf{r}) \int P_S\left(\mathbf{r}|\mathbf{r}', \Delta\right) e^{i2\pi\mathbf{q}(\mathbf{r}'-\mathbf{r})} d\mathbf{r}' d\mathbf{r} \qquad \textbf{Eq. 14}$$

By normalizing $\rho(\mathbf{r})$ and make the substitution $\mathbf{r}'-\mathbf{r} = \mathbf{R}$ the signal can be expressed as

$$S(\mathbf{q}) = \int P_S\left(\mathbf{R}, \Delta\right) e^{i2\pi\mathbf{q}\bullet\mathbf{R}} d\mathbf{R} \qquad \textbf{Eq. 15}$$

This follows the definition of the Fourier transform and determines the relation between the signal and the probability density distribution

$$S(\mathbf{q}) = FT\left(P_s\left(\mathbf{R}, \Delta\right)\right) \quad \textbf{Eq. 16}$$

If the inverse Fourier transform is applied on the signal attenuation curve the result will form a probability density distribution function.

$$FT^{-1}\left(S(\mathbf{q})\right) = P_S(R, \Delta) \quad \textbf{Eq. 17}$$

The probability density distribution describes how high the probability is for a molecule to have moved a specific distance during the diffusion time.

The full width at half maximum (FWHM) is the width of the probability density distribution at the half of the maximum and it represents the mean displacement of the molecules. If high enough q-values are not reached, the accuracy (resolution) of the determined FWHM will be to low. The trailing part of the signal versus q-curve (highest q-values) will correspond to the first part of the curve after the Fourier transformation, see Figure 5.

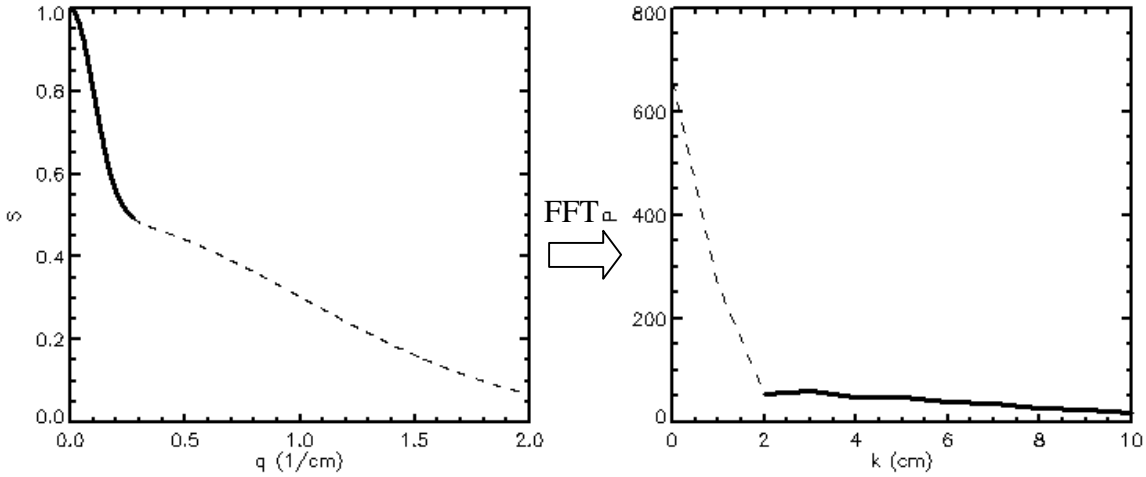

Figure 5 In the bi-exponential model the decay curve can be divided into two parts, represented by a thick solid line and a dashed line. The trailing part (dashed) prior to FT corresponds to the leading part after the Fourier transformation (right) and vice versa.

The root mean square displacement, Eq. 2, and the diffusion coefficient can be estimated from the FWHM value according to [3].

$$FWHM = 2\sqrt{4 \cdot D \cdot T_d \cdot \ln 2} \quad \textbf{Eq. 18}$$

$$s_{rms} = \sqrt{2 \cdot D \cdot T_d} = 0.425 \cdot FWHM \quad \textbf{Eq. 19}$$

The inverse of the maximum q-value will, after the Fourier transform, represent the distance between the sample points. The resolution after the Fourier transform can then be determined

$$\text{Resolution} = \frac{1}{q_{\max}} \quad \textbf{Eq. 20}$$

Since the signal attenuation curve is an even function [24] it can be mirrored, $S(q) = S(-q)$ and that gives the q-space resolution of the measurement [27]

$$\text{Resolution} = \frac{1}{2q_{\max}} \qquad \textbf{Eq. 21}$$

Hence, in a measurement situation, if the q-value are not high enough then the FWHM value will be overestimated [3] because the probability density distribution will be smeared out after that the signal attenuation curve has been Fourier transformed.

2.3.1 Restricted diffusion

When the T_d is sufficiently long the particles will collide in to the boundaries, they become restricted. To characterize the restriction a dimensionless variable, ξ, is defined according to

$$\xi = \frac{T_d D}{r^2} \qquad \textbf{Eq. 22}$$

where r is the diameter of the confinement i.e. the distance between the boundaries.

In the case of small T_d or large boundaries the particles will appear free, $\xi << 1$. When T_d is increased or the dimensions of the confinement decreased the particles becomes restricted, ξ approaches one and when the particles have bounced many times in the boundaries $\xi>1$, see Figure 6 [6]. With perfect reflecting walls the particle will be confined within the boundaries and completely restricted. The free diffusion is described by a Gaussian probability function whereas the restricted diffusion is non-Gaussian [21].

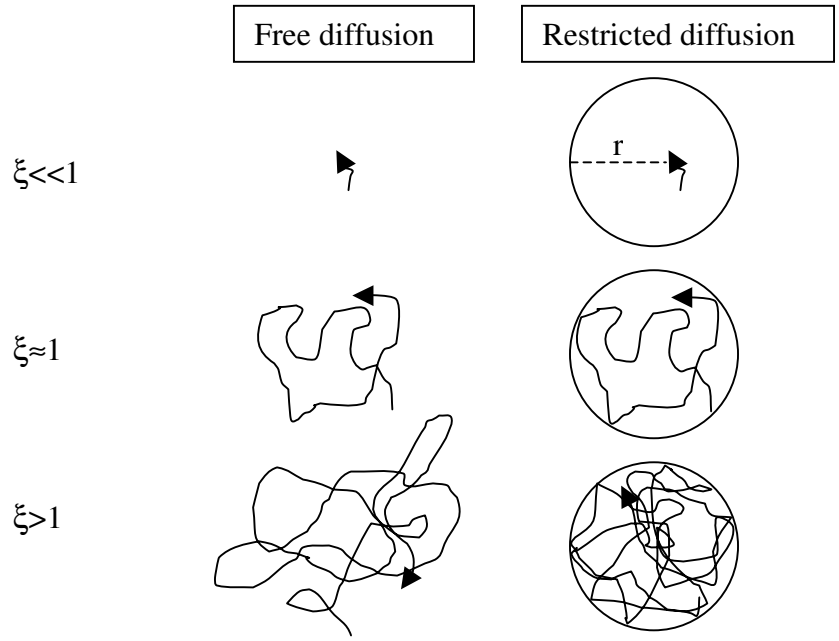

Figure 6 The path of a water molecule for different diffusion times from the case when the particle is free ($\xi<<1$) to when it is fully restricted ($\xi>1$).

The measured diffusion coefficient will be different depending upon if the water molecule is free or restricted. If the diffusion coefficient is measured in a restricted diffusion direction the value will be lower than if the diffusion coefficient is measured in a free diffusion direction.

The centre of mass (COM) of the path of a water molecule depends on how many time it have bounced in the walls. If the T_d is infinitesimal small ($\xi<<1$) the particle will not have time to move and the COM will be at the point where the water molecule is. When the T_d is increased the particle will bounce in the walls and the COM will move towards the centre of the confinement. If the T_d is infinite long the COM will be located in the centre of the confinement, see Figure 7

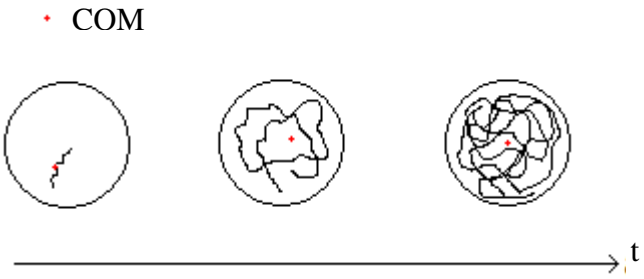

Figure 7 The centre of mass of the path a particle have moved will shift towards the centre of the confinement when the time, t, is increased. With sufficiently long time the centre of mass will be located in the middle of the confinement.

In biological tissues the boundaries are not absolute since the cell walls consist of a semi-parable membrane and the particles can pass through it. The probability for a particle to migrate thorough the membrane will increase with increasing measuring time and the particle will no longer be considered to be restricted, but only hindered. When a long T_d is used the water molecule is likely to penetrate through the semi permeable membranes and will appear to be free but in an apparently much more viscose substance [22].

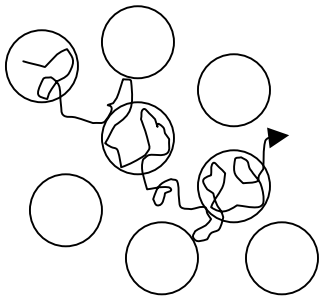

Figure 8 An illustration of the case when the boundaries are made of semi-parable membranes and the particle can migrate between the membranes.

An alternative theory, presented by Assaf *et al.* [23], is that hindered diffusion measured in biological tissue arises from the extra cellular fluid and is contributed to those water molecules that moves between the cells and only effects of the tortuosity that the cells or structures creates.

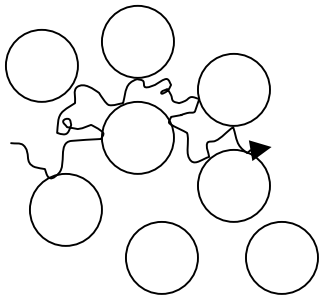

Figure 9 The hindered diffusion according to Assaf *et al.*[23]. The water molecule is moving between the cell structures.

2.3.2 Short gradient pulse (SGP) approximation

If the δ is so long that the motion of the molecule during δ not is neglecteble Eq. 13 is not valid. An error will be introduced and the measured distance during the diffusion time will be wrong. The result from the FWHM isn't true because of the movement during δ.

To avoid this, a condition for q-space analysis is the short gradient pulse (SGP) approximation, $\delta << \frac{a^2}{D}$ [18], where a is the confinement size. This approximation is possible to fulfil in the NMR environment where the gradient amplitudes are in the order of 10 T/m, but in clinical MRI this condition has to be violated in order to reach high enough q-values. This means that a q-space resolution better then 10 µm can be obtained, however, a high violation of the SGP condition is necessary.

2.4 Acquisition and post-processing

2.4.1 STEAM

STEAM (STimulated Echo Acquisition Mode) is a pulse sequence that utilises three 90° radio frequency (RF) pulses. The first pulse flips the spins into the xy-plane and there they will be labelled by a diffusion-encoding gradient. To give the spins time to move without loosing signal due to T2 relaxation the spins are then flipped back into the z-direction by the second 90° pulse. Back in the z-direction they are only affected by T1-relaxation. After a time, the mixing time (TM) the spins are flipped back to the xy-plane and the signal is read out by an EPI sequence after a refocusing of the diffusion encoding gradient.

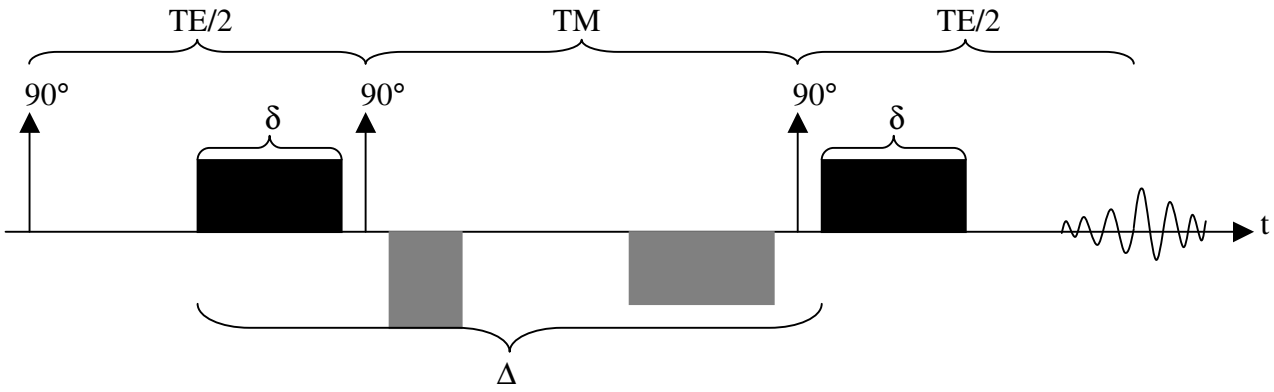

Figure 10 The STEAM pulse sequence, with three 90° pulses and two diffusion encoding gradient pulses (black). The two gradient pulses (grey) during the TM is used for compensation for Eddy currents and they also acts as spoiler gradients for signals excited by the second 90° pulse.

During the TM two additional gradient pulses are switched on (grey in Figure 10) in order to cancel Eddy currents caused by the diffusion encoding gradient pulses and to spoil signal contributions from the second 90° pulse. (Some of the spins have relaxed to the z-direction and when the second 90° pulse is turned on and they will be flipped down to the xy-plane. Some of the spins already in the xy-plane will not be affected of the second 90° pulse so to get rid of these signal components a spoiler is needed.)

2.4.2 Cross terms

When determining the diffusion sensitivity of pulse sequences one often applies the Stejskal-Tanner equation. This is however a simplification since all gradients within a pulse sequence will affect the b-value. In order to correctly determine the b-value, the double integral Eq. 23 will have to be solved, including all imaging gradients until the MR signal is collected.

$$b = \gamma^2 \int_0^{TE} \left(\int_0^{\tau} G'(t) dt \right)^2 d\tau \qquad \textbf{Eq. 23}$$

G' is the amplitude and τ is the duration of the gradients. By proper design of the pulse sequence, the effects of cross terms from imaging gradients can be minimised.

2.4.3 Eddy currents

When a magnet field gradient is switched on or off it will induce an electromagnetic force (emf) in the scanner according to Faraday's law of induction.

$$emf = -\frac{\partial \mathbf{\Phi}}{\partial t} = \int_{\Omega} \frac{\partial \mathbf{B}}{\partial t} d\mathbf{A} \qquad \textbf{Eq. 24}$$

The switching of a gradient creates an opposite magnetic field in the scanner that will affect the amplitude of the desired gradient. This leads to a distortion in geometric reconstruction of

the imaged object. The degree of the distortion varies with both the strength and orientation of the gradient pulse.

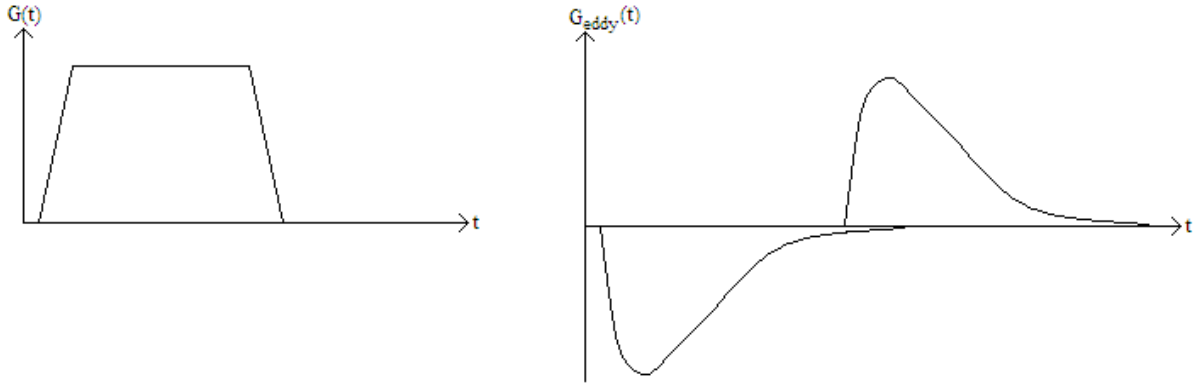

Figure 11 When a gradient (right) is switched on the positive slope will induce a negative eddy current (left) and when the gradient is switched off the negative slope will induce a positive eddy current.

2.4.4 Wavelet filtering

In order to compensate for low SNR present in highly diffusion weighted images, a wavelet filter can be aplied.

The measured MR signal consists of one imaginary and one real part. In order to perform wavelet filtering the signal is Fourier transformed and a Wiener-like filter is applied to the data. The filter is created from the input data and a combination of a hard threshold filter, HTF, $h_h(i,j)$

$$h_h(i,j) = \begin{cases} 1, \text{if } |y(i,j)| > \rho \cdot \sigma \\ 0, \qquad \text{otherwise} \end{cases} \qquad \textbf{Eq. 25}$$

where i and j is the pixel location, ρ is the threshold factor set by the user and σ is the standard deviation of the noise.

The outer part is a Wiener filter, WF, [28].

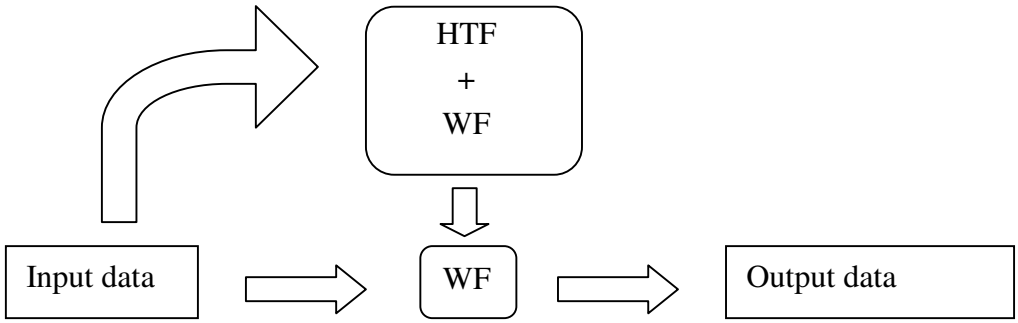

Figure 12 The input data is used to create a wiener-like filter based on a hard threshold and a Wiener filter. The Wiener like filter is then used on the input data to create the output data.

3 Method

In this project, two different effects were studied, namely how the FWHM is affected by different T_d:s and what effect different δ has on FWHM and $ADC_{lin\text{-}fast}$.

The first part consisted of simulations and *in-vivo* studies. The *in-vivo* measurements were performed in six healthy volunteers on a 3T Philips Achieva system with a maximum gradient strength of 63 mT/m. The simulations were performed as a random walk and simulated the COM and the signal attenuation curve so that D and FWHM could be determined.

The second part was carried out in six health volunteers using a Siemens Allegra 3T clinical head scanner with a maximum gradient strength of 40 mT/m.

3.1 Simulations

3.1.1 COM

To simulate the effect of the COM theory, a 10 µm box with perfectly reflecting walls was assumed and different diffusion encoding gradient durations were evaluated, δ = 7, 35, 200 ms. 10 000 particles were simulated for each δ and a COM was determined in two dimensions for every particle. A diffusion coefficient of $0.8 \cdot 10^{-9}\, m^2/s$ [29] was chosen to represent WM at 37°C.

3.1.2 D and FWHM

To determine D and FWHM different box sizes were assumed, box = 5, 10, 15, 20 and 50µm.

- T_d = 80 ms
- D = $2.5 \cdot 10^{-9}\, m^2/s$
- q_{max} = 889 cm^{-1}
- Number of q-values = 32

δ was varied between δ=0.01ms and 124 ms.

An additional simulation was performed with higher q-values, which was used to increase the q-space resolution. In the second simulation q_{max}=2222.5 cm^{-1} was assumed and this corresponds to a q-space resolution of 2.2µm. The FWHM was then determined.

3.2 In-vivo measurements with different δ

The 3T Philips Achieva system allows a maximum effective gradient strength of 89 mT/m when two directions are applied simultaneously (63mT/m on axis). A ramp time of 0.9 ms was used with a specially developed DW SE-EPI pulse sequence. Six healthy volunteers were scanned after that their informed consent was obtained. The volunteers consisted of two females and four males with a mean age of 28 years, ranging between 25 and 41 years.

Following measurement parameters were used:

- TR = 2000 ms
- T_d = 80 ms
- Slice thickness = 5 mm
- In plane resolution = 2.9×2.9 mm^2
- NEX = 4
- SENSE = 2

The TE varied between 124 and 148 ms when δ was varied between 24 and 42 ms (δ = 24, 30, 36, 42 ms). (Corresponding to a mean displacement distance of <x> = 11 to 14 µm for water molecules with D = $2.5 \cdot 10^{-9}\ m^2/s$)

For all measurements the q-value was varied from 0 cm^{-1} to 889 cm^{-1} in 12 steps.

For the measurement with different T_d the Siemens Allegra system with a STEAM pulse sequence was used with six diffusion encoding directions. Measurements were performed in six healthy volunteers after that their informed consent was obtained. The volunteer group consisted of four females and two males with a mean of 28 years raging between 22 and 41 years.

Following measurement parameters were used:

- TR = 2500 ms
- TE = 114 ms
- Slice thickness = 5 mm
- In plane resolution 1.81×1.81 mm^2
- NEX = 4
- δ = 43 ms

q was varied between 10 and 906 cm^{-1} in 12 equidistant steps for five different diffusion times (T_d = 64, 81, 100, 121, 144 ms). TM was maximised for each T_d to get a constant TE. To confirm the diffusion times and to examine any present effects of cross terms the sequence performance was evaluated in a water phantom.

3.3 Post-processing

In order to improve SNR all images from the Siemens Allegra were filtered with the wavelet method using a hard-threshold at 3.0 and all signal values below the noise level (mean value of a region of interest (ROI) in the background) were set to zero.

For all *in-vivo* measurements the signal decay curve was mirrored so that $S(q) = S(-q)$ and re-sampled to yield equidistant steps in q. No zero filling was used and this yielded a q-space resolution of 5.6 µm for the δ measurement and 5.5 µm for the T_d measurement (according to Eq. 21 [27]).

The $ADC_{lin\text{-}fast}$ value was determined from b= 0 s/mm^2 to 1200 s/mm^2, then by using the fast Fourier transformation (FFT), on the signal attenuation curve, the probability density distribution was obtained and the FWHM was determined. To obtain rotationally invariant parameters a tensor model was applied to the data (both $ADC_{lin\text{-}fast}$ and FWHM) and the largest and smallest eigenvalues, λ_1 and λ_3, were used to represent the parallel and the perpendicular diffusion direction.

Regions of interests (ROIs) were placed in the parametric maps of λ_1 and λ_3. For measurements with different δ the ROIs were positioned in the splenium of corpus calosum (scc, red), genu of corpus callosum (gcc, blue), and in gray matter (GM, green), see Figure 13.

For the measurements obtained with different T_d:s ROIs were positioned in grey matter (GM, green), posterior limb of the internal capsule (plic, red) and in genu of corpus callosum (gcc, blue), see Figure 14.

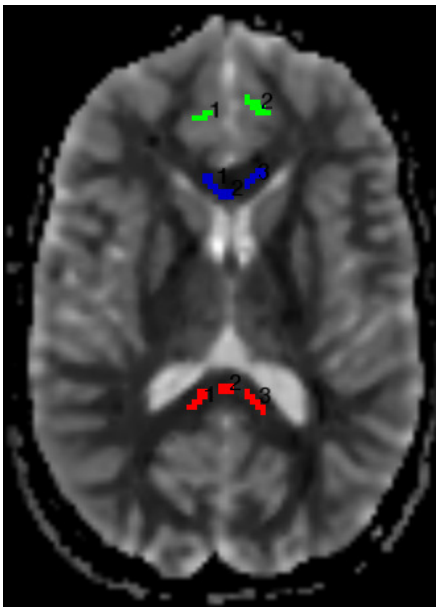

Figure 13 ROI placement in the volunteers for the measurement with different δ.

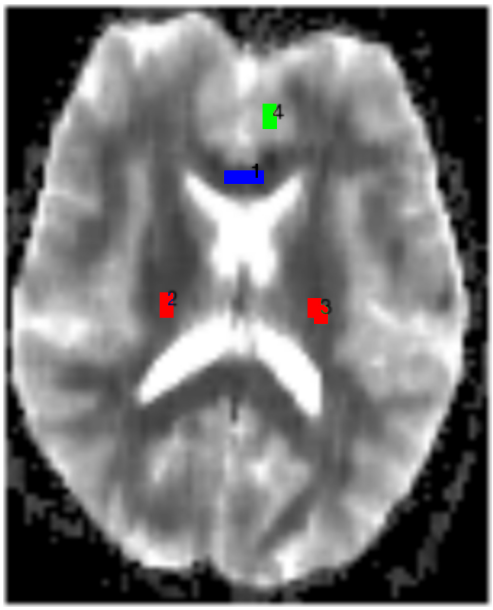

Figure 14 ROI places in the Td FWHM measurements.

4 Results

4.1 Simulations

4.1.1 COM

The simulation regarding the theory of COM clearly indicates that the COM will move towards the centre of the confinement when the duration of the diffusion encoding gradient is prolonged see Figure 15.

To the right in Figure 15 the profile of the COM is plotted, and it can be seen that the profile changes from an almost even distribution over the whole area to a normal distribution with increasing δ. For infinite small δ, the distribution will approach a straight line in the profile. The y-axis indicates the number of simulated particles that occupies a certain position, noted on the x-axis which represents the side of the simulated box (10 µm).

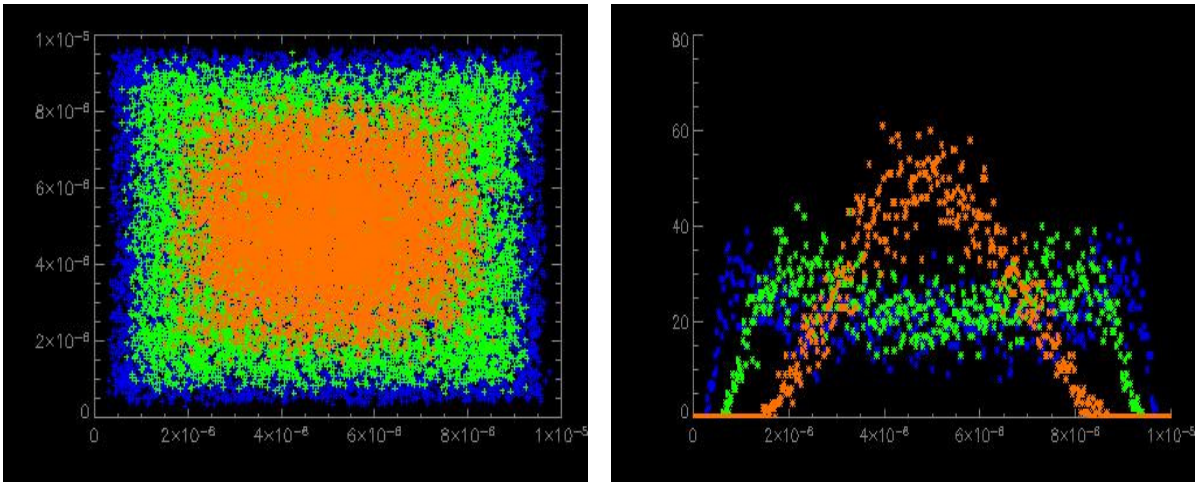

Figure 15 To the left a simulation of the COM, with δ=7, 35, 200 ms (blue, green and orange). The x axis represents the confinement which was 10 µm. To the right the profile of the same simulation is plotted and the number of simulated particles at a certain position is given by value on the y-axis.

4.1.2 D and FWHM

The simulation of D as a function of δ indicates that due to the COM theory, the observed D decreases with prolonged. The smallest deviation will be noted for the largest box (50 µm) while the largest deviation will be noted for the smallest box (5µm). The results are shown in Figure 16 where the normalised D is plotted as a function of δ all D-values are normalized to the measurement performed with δ = 21 ms in order to show the relative change in D.

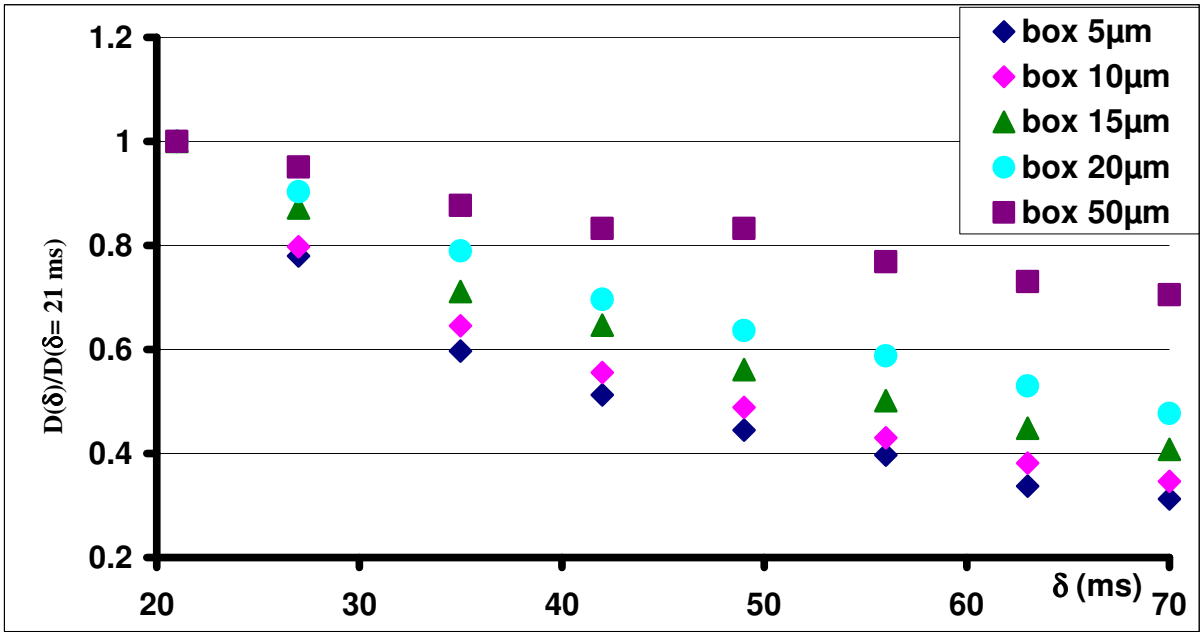

Figure 16 Result from the simulations of D, all values are normalized to the measurement with δ = 21 ms.

From the theory the expected effect on FWHM of a variation in δ is a declining FWHM and the largest effect is expected fore the smallest box. The obtained FWHM values shown in Figure 17 deviates from theory and the smallest box experiences the smallest effect of the increasing δ. The second simulation of FWHM, see Figure 18, shows that the result from Figure 17 is false and that it is an effect of poor q-space resolution. Even in Figure 18 the q-space resolution is too low to show the accurate effect of FWHM in the smallest box (5 µm) but the results from the simulation of the 10 µm box now better corresponds with the results obtained in the simulation of how the D value varies with varied δ. The q-space resolution with the high resolution is enough to resolve the FWHM in the 10 µm box.

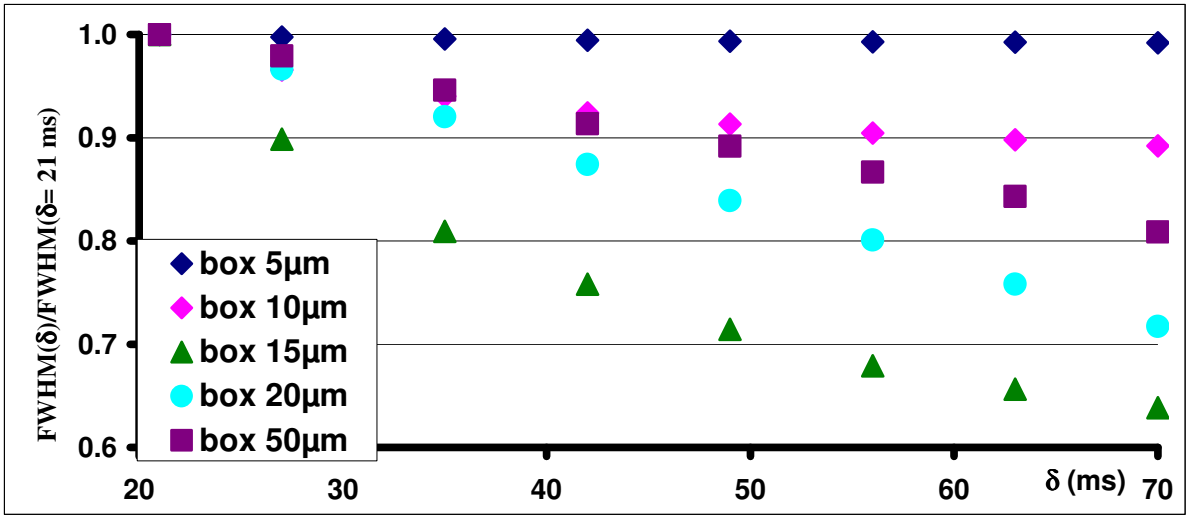

Figure 17 Simulation of FWHM, values are normalized to the measurement with δ = 21 ms. Notice the relative order of the data corresponding to different box sizes. The data corresponding to the smallest box (of 5 µm) does not appear to experience any changes with different δ followed by smaller changes for 10 µm box. The largest deviation is seen for the 15 µm box. The results apeares erroneously compared to the theory.

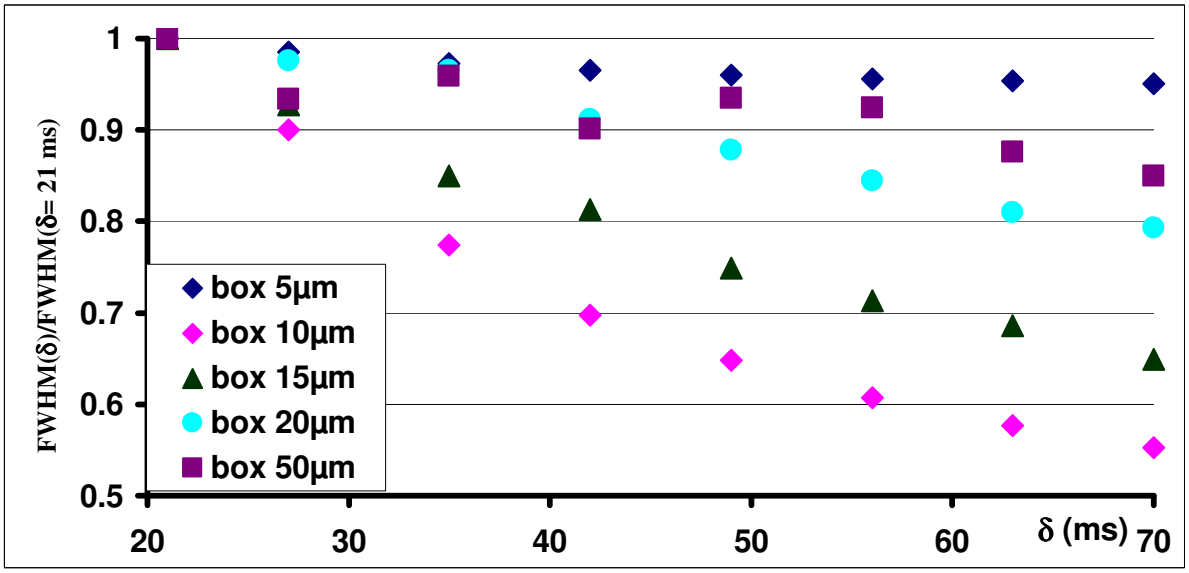

Figure 18 Second simulation of FWHM, values normalized to δ = 21ms. Notice the changed relative order of the data corresponding to different box sizes as compared to the results shown in Figure 17. The changes are due to the fact that a higher q-value was used in these simulations and therefore an increased q-space resolution was obtained. This clearly demonstrates that the q-space resolution affects the result.

4.2 Effects on ADC and FWHM of different δ

The measurements were performed at the Philips 3T Achieva in order to take advantage of the higher gradients and the better coil-performance as compared to the Siemens 3T Allegra. However, on the Philips system it was not possible to vary the duration of δ without simultaneously changing the TE. Hence, effects of a longer TE may also affect the results.

4.2.1 $ADC_{lin\text{-}fast}$

For WM, the fitted trend line $(ADC = k \cdot \delta + m)$ showed a small but noticeable decrease in eigenvalue one, λ_1.

In the diffusion direction orthogonal to the fibre direction (λ_3) the trend of ADC is almost the same in the different WM ROIs. The decrease or increase is so small that the trend can be considered constant and independent of δ. In WM gcc the slope was $k = -0.001$ and in WM scc the slope was $k = 0.002$ with the corresponding correlation coefficients $R = 0.78$ and $R = 0.84$, respectively. A decrease is supported by the simulations but at the same time it contradicts the result since the ADC, according to the simulations should be decreasing most in the direction with the least free space, *i.e.* in the direction orthogonal to the fibres.

The trend for GM is an increase in ADC for an increasing δ and the values are in the range between the values of λ_1 and λ_3 for WM.

The results are summarised in Table 1 and shown in Figure 19.

Table 1 Results from the measurements of $ADC_{lin\text{-}fast}$ obtained from six healthy volunteers on the Philips system. k is the slope of a linear trend line and R is the correlation coefficient. The data is given as (mean ± one standard deviation) [$\times 10^{-9}$ m^2/s].

δ	WM (gcc)		WM (scc)		GM	
(ms)	λ_1	λ_3	λ_1	λ_3	λ_1	λ_3
24	1.21±0.35	0.15±0.12	1.28±0.22	0.16±0.11	0.82±0.12	0.72±0.13
30	1.20±0.28	0.12±0.08	1.28±0.13	0.19±0.14	0.88±0.12	0.74±0.13
36	1.16±0.26	0.12±0.07	1.28±0.26	0.18±0.12	0.94±0.15	0.80±0.17
42	1.15±0.22	0.12±0.06	1.22±0.21	0.21±0.14	0.93±0.14	0.81±0.14
k	-0.004±0.0007	-0.001±0.0009	-0.003±0.0017	0.002±0.0009	0.001±0.0020	0.005±0.0011
R	0.92	0.78	0.77	0.84	0.92	0.97

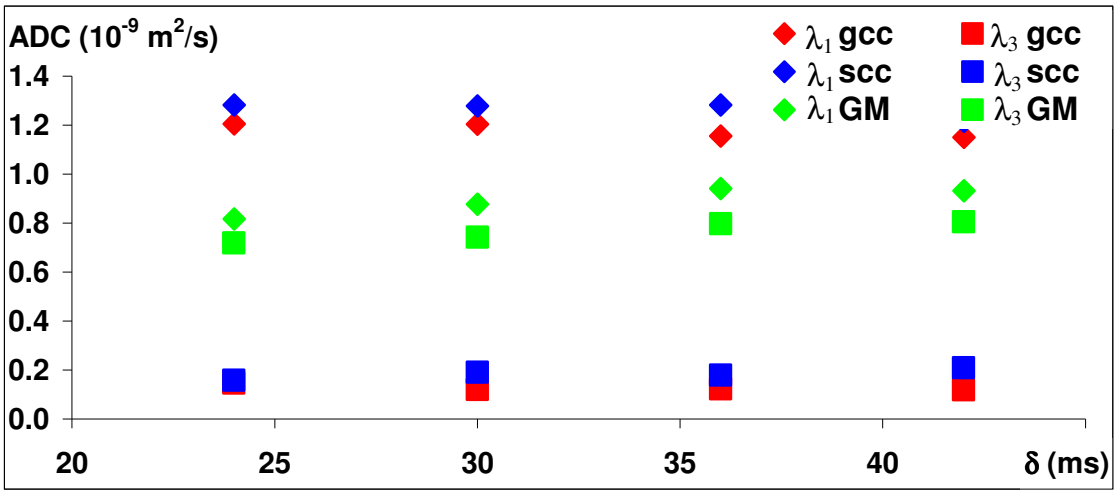

Figure 19 ADC as a function of δ, data corresponding to Table 1. A decreased ADC is noted for WM gcc and scc in the direction parallel to the fibre, λ_1. This was not expected but the trend have to be considered as accurate due to the correlation factor and the fact that both WM gcc and WM scc shows the same behaviour. The ADC-values obtained in GM is in the mid range between the values for the orthogonal and parallel diffusion direction in WM, the trend is an increase in ADC with increasing δ. The ADC in the direction orthogonal to the fibre direction is constant in the genu and splenium of the corpus callosum.

4.2.2 FWHM

In WM, for the most free direction a decreased FWHM is noticed with a slope of k = –0.16. For the diffusion direction orthogonal to the fibre direction the incline is zero or slightly positive, k = 0.02. For all λ_1 the correlation coefficient was high (R = 1.00 and 0.93, respectively) whereas for λ_3 the correlation coefficients was considerably less (R = 0.36 and R = 0.51, respectively). This means that the slope of λ_1 is more accurate than for λ_3 and a decrease in FWHM in the parallel fibre direction can be established.

In Figure 20 the values corresponding to the GM are found in the range between the λ_1 and λ_3 for WM and show almost the same trend, a small increase in FWHM with increasing δ.

The results are summarised in Table 2 and shown in Figure 20.

Table 2 Results from the measurements of the FWHM, performed on six healthy volunteers on the Philips system. k is the slope of a linear trend line and R is the correlation coefficient. The data is given in (mean ± one standard deviation) [µm].

δ	WM (gcc)		WM (scc)		GM	
(ms)	λ_1	λ_3	λ_1	λ_3	λ_1	λ_3
24	28.4±4.84	6.5±1.12	29.8±3.24	6.4±1.05	24.3±2.37	22.1±2.51
30	27.5±4.55	6.4±1.50	28.4±2.64	6.2±2.03	24.2±2.67	21.0±3.74
36	26.4±3.96	6.6±1.26	27.4±3.29	6.9±1.52	25.6±3.17	21.8±4.37
42	25.6±3.69	6.5±1.21	27.5±3.10	6.5±1.69	25.2±3.22	22.0±3.85
k	-0.16±0.006	0.00±0.007	-0.13±0.040	0.02±0.024	0.07±0.040	0.01±0.045
R	1.00	0.36	0.93	0.51	0.78	0.09

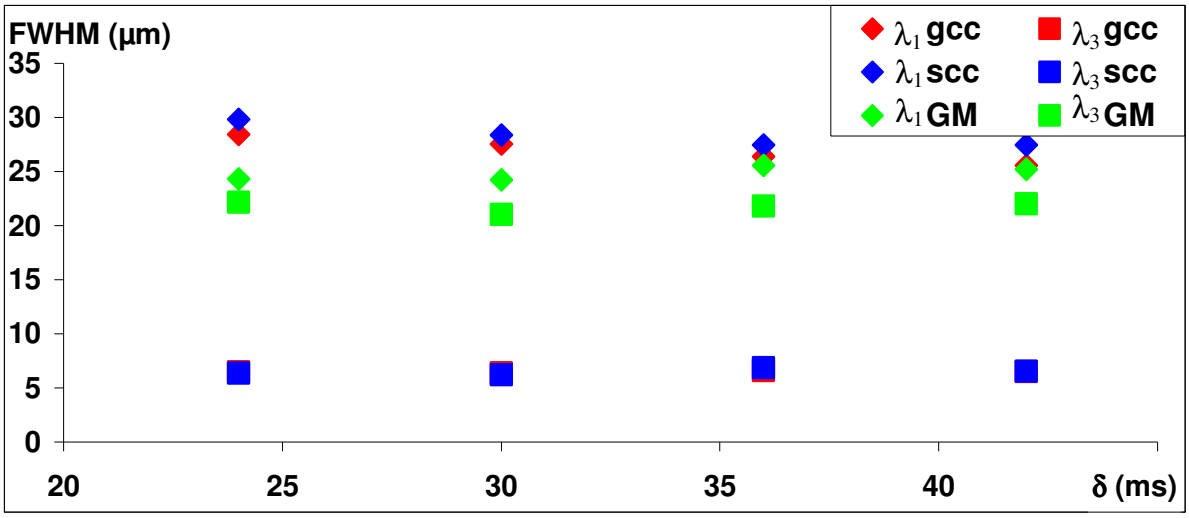

Figure 20 FWHM data corresponding to Table 2. In WM the FWHM is decreasing with increasing δ for λ_1. The trend is similar in both WM gcc and WM scc. Regarding λ_3, the slope is slightly positive.

4.3 Effects on FWHM of a varying T_d

The FWHM measured as a function of T_d reveals a clear difference between the diffusion direction parallel to the fibres and the diffusion direction orthogonal to the fibres. Similar results were obtained for both WM plic and WM gcc. In the direction parallel to the fibres the increase in FWHM was linear with the square root of T_d (Eq. 2). The same trend was observed for GM see Figure 21. A slight increase of FWHM-values was seen in the direction orthogonal to the fibres as well. The same trends were observed for GM see Figure 21.

For free diffusion a fitted trend line $(FWHM = k \cdot T_d + m)$ would give an interception of zero. In the most free diffusion direction, an intercept of 0.26 µm was obtained for WM plic (parallel to the fibre direction). For the parallel direction in WM gcc the intercept was −1.93 µm and for the orthogonal direction the intercept was –0.49 µm. In the direction orthogonal to the fibres the intercept was 2.82 µm for WM plic and this indicates that the diffusion is restricted in this direction.

Table 3 Results off the FWHM measurements performed on six healthy volunteers using a Siemens 3T system. The intercept is given by *m* and R is the correlation coefficient. Data is given as (mean ± one standard deviation) [µm].

$\sqrt{T_d}$ $(\sqrt{ms})$	WM (plic)		WM (gcc)		GM	
	λ_1	λ_3	λ_1	λ_3	λ_1	λ_3
8	25.9±2.62	8.4±0.45	30.4±3.38	8.5±1.26	25.9±1.93	19.0±2.28
9	28.1±3.85	9.0±1.07	36.1±4.28	7.9±1.90	29.3±1.95	22.4±2.43
10	30.1±3.70	10.1±0.93	38.4±4.71	9.3±3.16	32.0±2.89	24.2±2.99
11	33.3±4.70	10.3±1.39	42.3±5.71	10.3±3.06	35.6±2.53	27.0±3.60
12	38.8±5.58	11.3±1.73	47.7±6.62	12.5±1.88	40.5±1.84	29.8±4.21
m	0.26±4.112	2.82±0.707	-1.93±3.110	-0.49±2.750	-2.84±2.264	-1.82±1.229
R	0.97	0.98	0.99	0.91	0.99	1.00

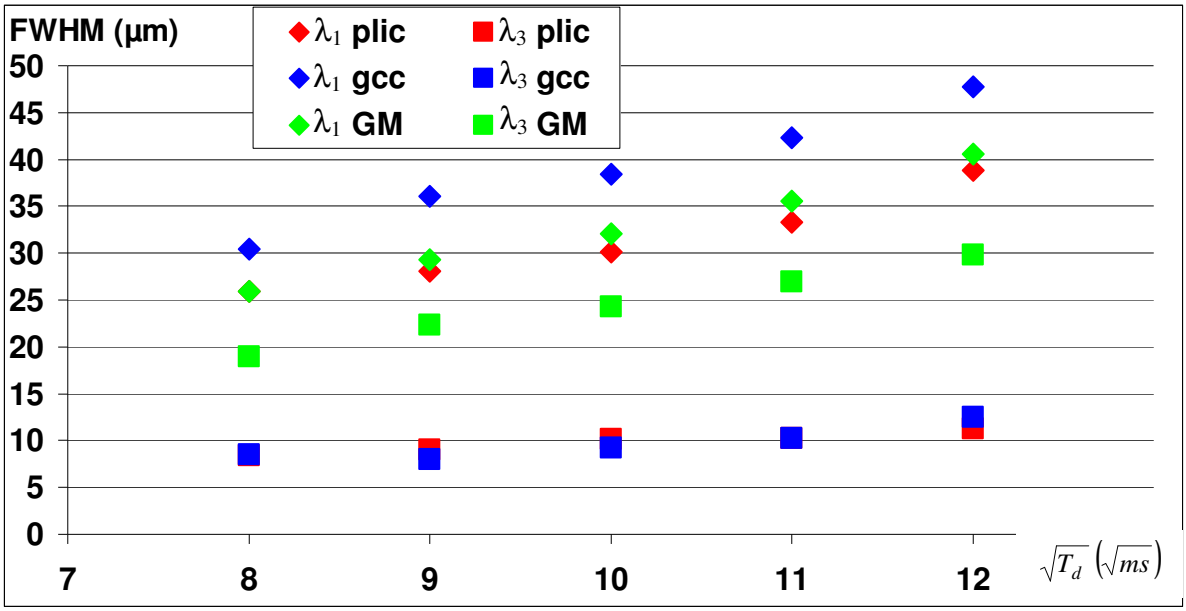

Figure 21 The FWHM values obtained for λ_1 (direction parallel to the fibres, ||) and λ_3 (direction orthogonal to the fibres) as a function of $\sqrt{T_d}$. The plotted data corresponds to Table 3 and shows a clear difference between λ_1 and λ_3. The FWHM for the direction parallel to the fibres is, as expected, increasing linearly with the square root of T_d and if the trend line is extrapolated to the intersect with the y-axis it will be close to zero for WM plic. The diffusion orthogonal to the fibre direction is clearly restricted; conclusion based on the deviation from zero in the m-value, and hence only shows a slight increase in FWHM, probably due to the semi permeable membranes.

5 Discussion

The effects of violating the SGP approximation on ADC and FWHM are to this day unknown. To some extent this have been done and a small decrease for the direction parallel to the diffusion encoding direction is noticeable for both FWHM and ADC when the degree of SGP violation is increased (δ is increased). In the diffusion direction orthogonal to the diffusion encoding direction the results is more uncertain, mostly due to poor q-space resolution and low SNR values.

When T_d was varied a clear difference between the direction parallel and the direction orthogonal to the diffusion encoding direction was noticed. This may indicates that the water in the orthogonal direction is restricted in some way and the water in the parallel direction is free. The water in the parallel direction is showing the same pattern as the water in the more anisotropic GM.

5.1 Effects on FWHM with use of a varying T_d

The results of this study show that there is a slight increase in FWHM in the diffusion direction perpendicular to the fibres (λ_3) when the diffusion time is increased, whereas the expected value, for a confinement with perfect reflecting walls should provide a constant FWHM [10], [16]. The slight increase may be explained by the fact that the water molecules migrate between the cell compartments through semi permeable membranes. When the diffusion is measured perpendicular to the fibre direction the contrast between WM and GM increase with increasing T_d, see Figure 21, which is in agreement with the results obtained by Nossin-Manor *et al.* [15]. In the diffusion direction parallel to the fibres the water is more free than in the diffusion direction perpendicular to the fibres and the FWHM is in the same order of magnitude as in GM. The increase of FWHM follows approximately a linear relationship with $\sqrt{T_d}$ as expected for free water, see Eq. 18.

In the GM, the water appears to be more free and there is no observed difference between λ_1 and λ_3. This indicates that the diffusion in GM is, as expected, less anisotropic than in WM [15].

In the case of free diffusion, the trend lines adopted to the λ_1 result in Figure 21 should intercept at zero when extrapolated to T_d=0 see Figure 22. In the case of restricted diffusion the corresponding extrapolation should not intercept at zero due to the restrictions. For short T_d the restriction does not have any effect and the particles will appear to be free, $\xi \ll 1$, see Eq. 22. When T_d is increased the restriction will affect the movement of the particles and the trend line will deviate from the free diffusion, $\xi > 1$.

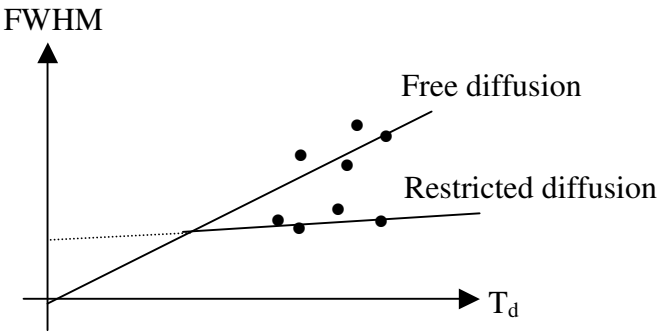

Figure 22 Extrapolating the trend lines from the measured data to T_d=0 provides information regarding if the diffusion is considered to be free or restricted. In the case of free diffusion the trend line is extrapolated to origo whereas in the case of restricted diffusion the intercept deviates from zero.

In Table 3 we can see that for the posterior limb of the internal capsule (plic) the trend line intercept, as expected, close to zero for λ_1 whereas for λ_3 in plic the intercept deviates from zero, indicating that it has to be restricted in some way, see Figure 22. Considering the genu of the corpus callosum (gcc), in contradiction to what was expected, the intercept for λ_1 deviated slightly from zero and was even closer to zero for λ_3. The result might be explained by a low SNR. The SNR for the data of gcc was much lower than for plic and this makes the result more uncertain. In plic the nerve fibres are oriented at a right angle to the slice direction so there will be no problem due to partial volume effects as long as the ROI is well inside the WM. In gcc, the nerve fibres are oriented parallel to the slice and the risk of partial volume effects becomes larger for thick slices. This means that it is considered safe to use a thick slice when the nerves are oriented orthogonal to the slice but not when the direction of the nerves bundles are in- plane.

5.2 Effects on ADC and FWHM of a varying δ

5.2.1 Simulations

In Figure 15 where the results of the COM simulation are shown. The results agree well with the expectation result that the COM is moving towards the centre of the confinement when the gradient duration time, δ, is increased [17]. In this simulation the barriers are perfectly reflecting walls, but if a parameter that permits a certain percentage of the molecules to pass through would be introduced, a similar result would be obtained but with a decrease in particles. When δ is long, the probability for a particle to escape the confinement will be higher due to the fact that the particle will be allowed to bounce in to the walls several times.

The simulation of how a measured D would be affected by a varying δ is shown in Figure 16. The D value is decreasing with increasing δ and for a smaller box the relative decrease is larger. The relative decrease is largest for the smallest box and smallest for the largest box due to the decreasing degree of restriction.

The corresponding simulation of FWHM is shown in Figure 17. In this case, the FWHM value is constant for the smallest box, probably since the q-space resolution is only 5.6 μm

which is larger than the actual box size (5 µm). The low q-space resolution will in this case result in an almost constant value of FWHM and the very small noted decrease is explained by the COM theory. Even for the box size of 10 µm the q-space resolution is a problem whereas for larger box sizes the q-space resolution was high enough. The highest q-value used for the simulation in Figure 17 was 889 cm^{-1} and corresponds to a q-space resolution of 5.6 µm. The q-value was chosen to represent the measurement performed at the Philips system (see chapter 3.2).

The second simulation was performed in order to examine whether the effect simulated in Figure 17 is an effect of the COM theory or an artefact due to poor q-space resolution. The obvious conclusion that can be drawn from Figure 18 is that the resolution may interfere with the FWHM value and "contaminate" the result. Even a q-space resolution of 2.2 µm is insufficient to correctly resolve the effect of COM in the smallest box (5 µm). The FWHM result from the 10 µm box has in this case changed and coincides with the expected value due to the COM theory, see Figure 18. The demonstrated resolution problem might become a potential problem for interpretations of the result for the *in vivo* measurements.

5.2.2 ADC

In the simulations the ADC value is determined from the simulated signal attenuation curve. The real measurements were performed in six diffusion encoding directions and hence a tensor model could be applied. From the tensor model, which allows, an approximation of the ADC values in all directions the largest ADC value (λ_1) and the smallest ADC value (λ_3) was extracted. For λ_3 (corresponding to the most restricted direction) the ADC value were constant in WM gcc and increasing in WM scc, but the data shows a larger correlation coefficient for WM gcc. According to the simulations, the ADC for the smallest confinement should decrease the most. The discrepancy between the simulations and the measurements may depend on cell boundaries. In the simulations, the boundaries are perfectly reflecting walls whereas *in vivo* they consist of semi permeable membranes. Additionally, in the simulations there were no other confounding factor such as e.g. a second diffusion coefficient which is believed to be present in the *in vivo* case. The result might also be explained by the fact that in this direction the δ does influence the results since already for the smallest δ (δ = 24 ms) the particles have reached the boundaries and are bouncing into the walls so often that the ADC value is as low as it's gets i.e. when δ is increasing the ADC value can't decrease any more. If δ is increased and are so long that the particles bounces many times in the boundaries the probability of the water molecules escape the confinement becomes so large that the water molecule appear free and the ADC then becomes constant. The same is expected in the direction parallel to the fibres (λ_1). In this direction the boundaries will not affect the particles since they are considered free. The results from the measurements are however showing a decrease in ADC.

The simulations of the ADC value is decreasing relatively more when the confinement is smaller than if the confinement is larger, compare 5 µm and 50 µm in Figure 16. This indicates that λ_3 will decrease more than λ_1 since λ_3 is the direction that represent the most

restricted direction and therefore have the smallest space to move in. The result might be explained by differences in the walls, in the simulation the walls are perfect reflecting and in the measurement the walls are semi-permeable. The semi permeability will allow the water molecules to pass and the effect of COM will not be as large as in the simulation.

For GM the result shown in Figure 19 presents a small increase in ADC. Eigenvalues one and three, are showing the same trend as λ_1 for WM but with different ADC values. The difference between λ_1 and λ_3 indicates that GM is less anisotropic than WM [15].

The pulse sequence protocol was designed to measure FWHM and not $ADC_{lin\text{-}fast}$. Further studies with a protocol with additional measuring points for lower b-values is needed to further investigate the effects on ADC with of a varying δ. Further more the ADC values were obtained using a linear fit described in Chapter 2.2.2. The bi-exponential fit that have been suggested in the literature [5], [31] are a favourite by many authors but is still controversial. The linear approximation was chosen because of the complexity of the bi-exponential fit. We estimated that the underestimation of $ADC_{lin\text{-}fast}$ relative to the bi-exponential method is equal for all δ and that the trend would be the same with the linear fit.

When comparing different data one should be aware of the fact that the SNR is different in different measuring points. An increased noise (decreased SNR) will add apparent anisotropy and lead to an underestimation of the diffusion tensor [30].

5.2.3 FWHM

The expected FWHM for λ_1, when δ is increased, is a constant value since T_d is constant. This expectation was not in agreement with the result obtained from the measurements, see Figure 20. The result indicates that there is a restriction even in the parallel direction.

In the most restricted direction (λ_3) the FWHM value was almost constant. This was in agreement with the first simulation of FWHM and a box of approximately 5 µm in Figure 17 where the FWHM was constant probably due to a poor q-space resolution. The box is smaller than the q-space resolution and this poses a problem. To compensate for the poor q-space resolution the tensor model can be used. Using the tensor model we can resolve smaller objects than the spatial resolution, since the model provides data that is fitted from many measurements. See Appendix B. The measured FWHM value of approximately 7 µm can then still be the restriction that the water molecules “feel”, even if it is close to the q-space resolution and the simulations point towards that this is a much to poor q-space resolution.

Both the T_d and the δ results are preliminary and further studies are needed to establish the effect of different δ and T_d.

6 Conclusion

The result of the FWHM measurement obtained with varying T_d indicates a restriction in the direction perpendicular to the fibres in white brain matter.

To optimise T_d one has to decide what the goal of the measurement is. If the goal is to measure the size of the confinement T_d should be as small as possible in order so that the effect of water molecules migrating over the cell membrane is minimised. The T_d should also be so long that all of the confinement is sampled. If the confinement is in the magnitude of 10 µm, then the time should be approximately 20 ms according to Einstein's equation, Eq. 2. If the goal is a high contrast between WM and GM, the T_d should be longer since the FWHM values for WM and GM is diverging, see Figure 21.

When values from diffusion measurements are compared between clinics, notice is normally not taken to different diffusion encoding gradient duration, δ, and ADC and FWHM are considered to be independent of δ. Based on the findings in this preliminary study, sequence parameters ought to be considered when comparing measurements are carried out at different sites. Even if the changes are not huge, the COM theory will affect the values and δ should be kept as low as reasonable achievable. The effect on ADC and FWHM when δ is doubled is a decrease with approximately 10 % in FWHM and 5 % in ADC. To establish the decrease further investigation is needed.

In the most restricted direction the ADC and FWHM values are constant and no notice have to be taken to the duration of δ.

Most MRI systems today are not capable of resolving structures *in vivo*. The problem with low q-values and hence low q-space resolution can not be avoided despite the use of the tensor model to estimate the structure sizes in the brain. Some of the smallest structures may be hard or even impossible to measure and as the result shows so can the FWHM values obtained in the most restricted direction not be trusted due to the poor q-space resolution.

Acknowledgements

I would like to express my gratitude to the people how made this thesis possible. All of the MR-physics group, at Lund University hospital, for the inspiration to work with MRI and to stay in this line of research. A special big thanks to my supervisors Sara Brockstedt, Jimmy Lätt and Markus Nilsson. They have all been of great help and have shown a tremendous patience with all questions all of their working day and even late at night. Even if Jimmy and Markus will like to emphasise that they only were resource persons they have been like supervisor to.

My friend, college and colour coordinator Anna Rydhög have had big part in this thesis too. For all the discussions we have hade to complete this thesis and all the fun we have had while writing them.

I would also like to thank professor Freddy Ståhlberg. His support and good idéa's have raised the quality of this work and the abstract sent to ISMRM.

Last but not least I would like to thank all the volunteers that have been so kind to let me have a small part of their time to take some images. You have all been great and have taken part of the study without any compensation, without you this would not have been possible.

Emil Nordh

Lund, 19th of February, 2007

Bibliography

[1]. Nobel Foundation, http://nobelprize.org/nobel_prizes/medicine/laureates/2003/press-sv.html, [Online; accessed 2006-12-11]

[2]. M. E. Moseley, K. Butts, M. A. Yenari, M. Marks, A. de Crespigny, *Clinical aspects of DWI*, NMR in Biomed, 8**:** 387– 396 (1995)

[3]. Y.Cohen, Y. Assaf, *High b-value q-space analysed diffusion-weighted MRS and MRI in neuronal tissues – a technical review*, NMR Biomed. 15:516-542 (2002)

[4]. C. A. Clark, D. Le Bihan, *Water Diffusion Compartmentation and Anisotropy at High b Values in the Human Brain*, MRM 44:852-859 (2000)

[5]. C. A. Clark, M. Hedehus, M. E. Moseley, *In Vivo Mapping of the Fast and Slow Diffusion Tensor in Human Brain*, MRM 47:623-628 (2002)

[6]. William S. Price, *Pulsed-Field Gradient Nuclear Magnetic Resonance as a Tool for Studing Translation Diffusion: Part 1. Basic Theory*, Concepts Magnetic Resonance 9:299-336, (1997)

[7]. P. C. M. van Zijl, C. T. W. Moonen, P. Faustino, J. Pekar, O. Kaplan, J. S. Cohen, *Complete separation of intracellular and extracellular information in NMR spectra of perfused cells by diffusion-weighted spectroscopy*, Natl. Acad. Sci. USA 88:3228-3232 (1991)

[8]. C. H. Sotak, *Nuclear magnetic resonance (NMR) measurement of the apparent diffusion coefficient (ADC) of tissue water and its relationship to cell volume changes in pathological states*, neuint 45:569-582 (2004)

[9]. A. Schwarcz, P. Borgner, P. Meric, J-L. Correze, Z. Berente, J. Pál, F. Gallyas, T. Doczi, B. Gillet, J-C. Beloeil, *The Existence of Biexponential Signal Decay in Magnetic Resonance Diffusion-Weighted Imaging Appears to Be Independent of Compartmentalization*, MRM 51:278-285, (2004)

[10]. D. Topgaard, O.Söderman, *Experimental determination of pore shape and size using q-space NMR microscopy in long diffusion-time limit*, MRI 21:69-76 (2003)

[11]. G. E. Weseby, M. E. Moseley, R. L. Ehman, *Translation molecular self-diffusion in magnetic resonance imaging: II. Measurement of the self-diffusion coefficient*, Invest. Radiol 19: 491-498 (1984)

[12]. D. Le Bihan, E. Breton, *In vivo magnetic resonance imaging of diffusion*, C. R. Acad. Sc. Paris, 15:1109-1112 (1985)

[13]. D. Le Bihan, E. Breton, D. Lallemand, P. Grenier, E. Cabanis, M. Laval-Jeantet, *MR imaging of intravoxel incoherent motions: Application to diffusion and perfusion in neurologic disorders*, Radiology 161:401-407 (1986)

[14]. P. Callaghan, D. MacGowan, K.J. Packer, F.O. Zelaya, *Influence og field gradient strength in NMR studies of diffusion in porous media*, MRI 9:663-671 (1991)

[15]. R. Nossin-Manor, R. Duvdevani, Y. Cohen, *Effect of Experimental Parameters on High b-Value q-Space MR Images of Excised Rat Spinal Cord*, MRM 54:96-104 (2005)

[16]. H. Wassenius, M. Nydén, B. Vincent, *NMR diffusion studies of translational properties of oil inside core-shell latex particles*, JCIS 264:538-547 (2003)

[17]. P.P. Mitra, B.I. Halperin, *Effects of Finite Gradient-Pulse Widths in Pulsed-Field-Gradient Diffusion Measurements*, JMR, Series A, 113:94-101 (1995)

[18]. C. Malmborg, D. Topgaard, O. Söderman, *NMR diffusometry and the short gradient pilse limit approximation*, JMR 169:85-91 (2004)

[19]. C. Malmborg, M. Sjöbeck, S. Brockstedt, E. Englund, O. Söderman, D. Topgaard, *Mapping the intracellular fraction of water by varying the gradient pulse length in q-space diffusion MRI*, JMR 180:280-285, (2006)

[20]. Y. Assaf, D. Ben-Bashat, J. Chapman, S. Peled, I.E. Biton, M. Kafri, Y. Segev, T. Hendler, A.D. Korczyn, M. Graif, Y. Cohen, *High b-Value q-Space Analyzed Diffusion-Weighted MRI: Application to Multiple Sclerosis*, MRM 47:115-126 (2002)

[21]. Y.Assaf, P J. Basser, *Composite hindered and restricted model of diffusion (CHARMED) MR imaging of the human brain*, NeuroImage 27:48-58 (2005)

[22]. D. Topgaard, C. Malmborg, O. Söderman, *Restricted Sefl-Diffusion of Water in a Highly Concentrated W/O Emulsion Studied Using Modulated Gradient Spin-Echo NMR*, JMR 156:195-201 (2002)

[23]. Y. Assaf, R Z. Freidlin, G. Rohde, P J. Basser, *New Modeling and Experimental Framework to Characterize Hindered and Restricted Water Diffusion in Brain White Matter*, MRM 52:965-978 (2004)

[24]. E. O. Stejskal, J. E. Tanner, *Spin diffusion measurements: spin echoes in the presence of a time dependent field gradient*, J. Chem. Phys. 42:288-292 (1965)

[25]. P. B. Kingsley, *Introduction to Diffusion Tensor Imaging Mathematics: Part II. Anisotropy, Diffusion-Weighting Factors, and Gradient Encoding Schemes*, Concepts Magn Reson Part A 28 A:123-154 (2006)

[26]. P. T. Callaghan, *Principles of Nuclear Magnetic Resonance Microscopy*, Clarendon Press 1993 ISBN 0 19 853997 5

[27]. C.-P. Lin, V- J. Wedeen, J.-H. Chen, C. Yao, W.-Y. I. Tseng, *Validation of diffusion spectrum magnetic resonance imaging with manganese-enhanced rat optic tracts and ex vivo phantoms*, NeuroImage 19:482-495 (2003)

[28]. A. Bibic, *Denoicing of Complex MRI Data by Wiener-like Filtering in the Wavelet Domain: Application to High b-value Diffusion Weighted Imaging*, Degree project 20 credits in medical radiation physics. Spring 2005 Departent of Medical Physics, Lund University.

[29]. S. Brockstedt, C. Thomsen, R. Wirestam, S. Holtås, F. Ståhlberg, *Quantitative Diffusion Coefficient Maps Using Fast Spin-Echo MRI*, MRI 16:877-886 (1998)

[30]. D. K. Jones, P. J. Basser, *"Squashing Peanuts and Smashing Pumpkins:": How Noise Distorts Diffusion-Weighted MR Data*, 52:979-993 (2004)

[31]. S. E. Maier, S. Vajapeyam, H. Mamata, C-F. Westin, F. A. Jolesz, R. V. Mulkern, *Biexponential Diffusion Tensor Analysis of Human Brain Diffusion Data*, MRM 51:321-330 (2004)

Appendix A

Signal decay for δ measurements

Philips

Table 4 Signal decay from q=0 cm^{-1} to q=889 cm^{-1}. The mean of the signals for the two last q-values have been divided by the signal for q=0 cm^{-1}. The smallest signal decay of all six directions and all ROIs is noted in the table.

δ (ms)	WM (%)	GM (%)
24	82.8	97.5
30	82.2	97.0
36	79.5	96.8
42	79.8	97.1

Appendix B

Tensor measurement example

As an example a 2D tensor is fitted to the measuring points in Figure 23. The tensor is described by the 2×2 matrix in Eq. 26 and the values on the tensor (black line) can then be calculated from Eq. 26. The red circle in Figure 23 is the q-space resolution, given by Eq. 21 depending on q_{max}, and by fitting a tensor to the measurements information about points inside the q-space resolution is given.

$$\begin{pmatrix}\cos\theta & \sin\theta\end{pmatrix}\begin{pmatrix}1 & 0\\ 0 & 0\end{pmatrix}\begin{pmatrix}\cos\theta\\ \sin\theta\end{pmatrix} \qquad \text{Eq. 26}$$

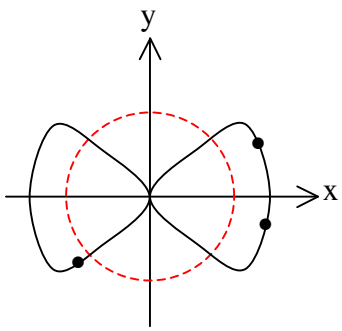

Figure 23 To the measured points (black dots) a tensor is fitted (black solid line). The tensor have the shape of a peanut in the 2D example. The red dashed circle is the q-space resolution and the tensor gives information about points inside the q-space resolution.

Appendix C

Abstract ISMRM

Does changes in gradient duration influence q-space-based determinations of displacement in vivo?

E. Nordh[1], J. Lätt[1], M. Nilsson[1], A. Rydhög[1], S. Brockstedt[1], and F. Ståhlberg[1]
[1]Medical Radiation Physics, Lund University, Lund, Sweden

Introduction

The aim of this study was to evaluate the effect when violating the Short Gradient Pulse (SGP) approximation and its effect on FWHM. The evaluation was done on a clinical 3T MRI scanner, using a specially developed diffusion weighted SE-EPI pulse sequence. We hypothesised that it is possible to visualise the effect of violating the SGP, and thereby indirect visualize structural sizes and permeability of the cell membranes that constitute the confining diffusion geometry *in vivo*.

Theory

In q-space imaging a short diffusion encoding gradient pulse duration δ is assumed [1]. Violation of the condition $\delta \ll \Delta$ leads to an under estimation of measured structural size. With a clinical scanner, this condition it is rarely possible to fulfil since δ needs to be relatively long to achieve sufficiently high q-values. When δ increases the water molecules will get a phase shift correlated to the Centre of Mass (COM) of the path they have travelled during the time δ. For large δ, the water molecules are reflected by the barriers of the confining geometry and the COM will approach the centre of the geometry and it will hence be less likely for the water molecules to have its COM close to the pore walls [2]. This assumption of COM is only valid when the structure walls are perfectly reflecting.

Materials and Methods

This study was preformed *in-vivo* at a 3T Philips Achieva system with a maximum effective gradient strength of 89 mT/m using a SE-EPI sequence. Three healthy volunteers were scanned after their informed consent was obtained. q-Space data was sampled in six directions with q varying from 0 to 889 cm^{-1} in 12 steps. To gradually increase the violation of the SGP, measurements were made with δ = 24, 30, 36 and 42 ms and a diffusion time T_D = 80 ms. The repetition time (TR) was 2000 ms and the echo time (TE) was varied from 124 ms to 148 ms as δ varied. Pixelwise calculations were performed and for each pixel the S(q) curve was re-sampled to 24 data points to yield equidistant steps in q and then mirrored so that S(-q) = S(q), giving a nominal resolution of 5.6 μm [2]. After calculation of the Full Width at Half Maximum (FWHM) of the displacement probability in each direction, a tensor analysis was performed [4]. The largest eigenvalue λ_1 and the smallest eigenvalue λ_3 of the tensor then provided the FWHM in the most restricted and most unrestricted direction, respectively. In the parametric maps of λ_1 and λ_3 regions of interest (ROI) were positioned in the splenium of corpus calosum (scc, red), genu of corpus callosum (gcc, blue), and in gray matter (GM, green), see figure 1. In order to verify the obtained result a simulation of a random walk was performed. Perfectly reflecting planes were assuming, separated a distance = 5, 10, 15, 20 and 50 μm. The diffusion encoding parameters were the same as in the *in vivo* protocol. The simulation was performed without noise.

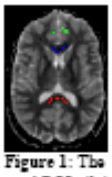

Figure 1: The used ROIs (λ_1)

Results

Table 1 shows the obtained FWHM values, with a slight declining trend both in scc and gcc for both eigenvalue one (λ_1) and three (λ_3). Figure 2 shows the result from the simulation.

δ	Scc		Gcc		GM	
(ms)	λ_1	λ_3	λ_1	λ_3	λ_1	λ_3
24	35.8±3.4	7.4±0.6	35.6±2.6	7.0±0.5	24.1±1.3	21.4±1.4
30	34.6±2.6	7.1±0.5	34.9±1.2	6.6±0.5	24.6±1.4	21.2±1.6
36	33.2±0.9	7.1±0.5	33.0±0.9	6.6±0.6	25.8±0.6	21.7±1.3
42	33.5±12	7.0±0.5	31.8±1.8	6.4±0.6	25.6±1.3	21.9±2.1
k / R	-0.14 / 0.9	-0.02 / 0.9	-0.22 / 1.0	-0.03 / 0.9	0.10 / 0.9	0.03 / 0.8

Table 1: The obtained FWHM from the ROIs in WM and GM. The given standard deviation correspond to the deviation between results from experiment. The data for δ is given in mean ± Standard Deviation, k=slope and R=correlation coefficient for the linear approximation fitted to the measured values.

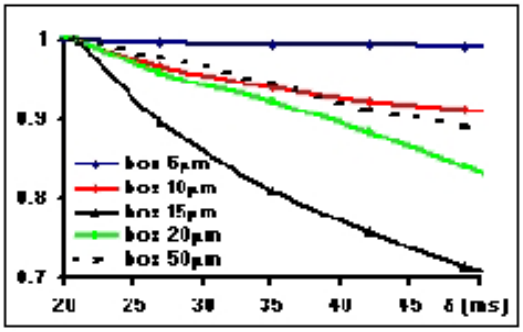

Figur 2: Obtained FWHM values, normalised for δ=21 ms. It can be seen that the smallest decline is obtained with the smallest box size, due to the asymptotic behaviour when violating the SGP to a different degree.

Discussion

A slight decrease of FWHM for increasing δ, was found for both λ_1 and λ_3. In the most restricted direction, λ_3, this result is expected from the COM theory as well as from the simulations. Assuming a confined geometry of 5 μm and δ=[22-42] ms, the violation of SGP is so severe that only a slight decrease in FWHM is expected. This result is also in agreement with the NMR spectrometer results of Nossin-Manor [6] who found a small decrease in the mean displacement (proportional to FWHM) orthogonal to the fibres with δ = 2 and 20 ms. However, in our results we see a decrease also in the largest eigenvalue λ_1. This possibly indicates effects of a restriction in the diffusion also parallel with the fibres. The simulations might suggest such an interpretation, since the effects of the violation of the SGP would be more pronounced for a larger confining geometry than for a smaller. In conclusion, small but observable changes in FWHM are seen, indicating that the "severity of violation" of the SGP condition has a minor influence on the measured parameter FWHM when changing δ in the range studied in this work.

The authors acknowledge Philips Clinical Science for assistance with sequence development.

Reference

[1]. P.T. Callaghan, *et al.* JMR (1990), 90:177-182
[2]. C. Malmborg, *et al.* JMR (2006) 180:280-285
[3]. C-P Lin, *et al.* Neuro Image (2003) 19:482-495
[4]. Y. Assaf, *et al.* MRM (2002) 47:115-126
[5]. R. Nossin-Manor, *et. al.* MRM (2005) 54:96-104

Appendix D

Abbreviations

ADC	Apparent Diffusion Coefficient
COM	Centre of Mass
D	Diffusion coefficient
DWI	Diffusion Weighted Imaging
DTI	Diffusion Tensor Imaging
EPI	Echo Planar Imaging
FFT	Fast Fourier Transformation
FOV	Field of View
FWHM	Full Width at Half Maximum
gcc	genu of corpus callosum
GM	Grey Matter
MRI	Magnetic Resonance Imaging
MSD	Mean Square Distance
NEX	Number of Excitation
NMR	Nuclear Magnetic Resonance
plic	posterior limb of the internal capsule
Rms	Root Mean Square
ROI	Region of Interest
SC	Spinal Cord
scc	splenium of corpus callosum
SE	Spinn Echo
SGP	Short Gradient Pulse
SNR	Signal to Noise Ratio
STEAM	Stimulated Echo Acquisition Mode
T_d	Diffusion time
TE	Echo Time
TM	Mixing Time
TR	Repetition Time
WM	White Matter

Appendix E

Svensk populärvetenskaplig sammanfattning

Emil Nordh

Har mättiden någon inverkan på resultatet vid diffusionsmättningar med magnetresonanstomografi (MRT)?

Vattenmolekyler är i ständig slumpmässig rörelse som beror på systemets termisk energi, dvs temperaturen. Diffusionsrörelsen kallas även Brownsk rörelse efter den engelske botanikerns Brown, som upptäckte fenomenet på 1800 talet.
Människokroppen består till 70 % av vatten, vilket gör det lämpligt att använda MRT för att studera diffusionsegenskaper i biologisk vävnad och för klinisk diagnostik av ex. akut ishemisk stroke eller för studier av sjukdomar som påverkar hjärnans vita substans så som demens och multiple skleros.

Då man tar en diffusionsbild med MRT använder man två extra diffusionskodande magnetfältspulser, utöver de som används för själva bildtagningen. Då olika vattenmolekyler känner av olika starka magnetfält kan man detektera diffusionsrörelsen, som normallt inte är mer än ca 10-50 mikrometer vid normal kroppstemperatur, genom så kallad fasdispersion. Hastigheten på vattnets slumpmässiga rörelse bestäms av dels av cellernas genomsläplighet i kroppen samt av hur länge vi studerar diffusionsrörelsen. Genom att bestämma den skenbara diffusionshastighet som uppkommer till följd av att olika vävnadstyper har olika egenskaper, kan man generera bilder som används i den kliniska verksamheten. En viktig tillämpning inom diagnostiken är att lokalisera blodproppar i hjärnan vid s.k. hjärninfarkt. Beroende på orsaken sätts olika behandlingar in, därav är det viktigt att fort ställa rätt diagnos. Idag är diffusionsviktad MRT den enda bilddiagnostikmetoden där man kan urskilja proppen i ett akut skede.

Denna studie syftar till att studera om och i så fall hur stor effekt den faktiska mättiden av diffusionsrörelsen har. Dels undersöktes effekterna av varaktigheten av de extra diffusionkodande magnetfältetspulsen har och dels effekterna av tidsskillnaden mellan dem, d.v.s. diffusionstiden. Diffusionstiden som studerades ligger mellan 50 till 150 millisekunder. Utvärderingen gjordes med s.k. q-space analys vilket är en analysmetod som framför allt används inom fysikaliskkemi för att studera strukturella storlekar av exempelvis protoner. Från q-space analysen utvärderades måttet på hur långt vattenmolekylerna utbreder sig under diffusionstiden d.v.s. FWHM (full width at half maximum). Om vattnet skulle vara hindrat i någon riktning (begränsa till en cell) skulle FWHM vara oberoende av diffusionstiden så snart mättiden är tillräckligt lång för att vattenmolekylerna ska hinna slå i cellväggarna. Vid en sådan situation skulle FWHM kunna användas för att mäta cellstorlekar inne i kroppen.

När man jämför diffusionsbilder mellan kliniker idag anser man att den uppmätta diffusionshastigheten inte påverkas av hur lång tid de diffusioninkodande pulserna varit påslagna. Resultat av denna studie visar att det möjligen finns ett samband och att man underskattar diffusionsrörelsen då de diffusioninkodande pulserna är påslagna under en relativt lång tid.

Den andra parametern som har undersökts är hur FWHM varierar med själva diffusionstiden. Resultatet visar att vattnet är hindrat i sin diffusion i vissa cellriktningar och FWHM blir i stort sett konstant vid mätningar tvärs fiberriktningnen i vit hjärnvävnad. För mätningar längs med fiberriktningar visar FWHM en svag ökning, vilket möjligen kan bero på att cellernas membran är genomsläppligt för vattenmolekyler under de tider som vi studerar diffusionsförloppet.

Handledare: **Sara Brockstedt, Jimmy Lätt**
Examensarbete 20p i Medicinsk Strålningsfysik Ht 2006
Avdelningen för medicinsk strålningsfysik, Lunds Universitet